Electronic Supplementary Material

Facile synthesis of fluorescent hetero[8]circulene analogues with tunable solubilities and optical properties

Yusuke Matsuo, Fengkun Chen, Koki Kise, Takayuki Tanaka* and Atsuhiro Osuka

Department of Chemistry, Graduate School of Science, Kyoto University, Sakyo-ku, Kyoto 606-8502, Japan.

E-mail: taka@kuchem.kyoto-u.ac

Contents

1. Instrumentation and Materials

Commercially available solvents and reagents were used without further purification unless otherwise noted. 2,5-bis(2-bromophenyl)-1*H*-pyrrole[S1], 5-methoxy-2-(4,4,5,5-tetramethyl-1,3,2-dioxaborolan-2-yl)-1*H*-indole[S2] and 5-chloro-2-(4,4,5,5-tetramethyl-1,3,2-dioxaborolan-2-yl)-1*H*-indole[S2] were prepared according to the reported procedures, respectively. Dry dichloromethane was purchased from Wako Pure Chemical Industries, Ltd. Dry tetrahydrofuran (THF) was obtained by passing through alumina under N_2 in a solvent purification system. The spectroscopic grade solvents were used as solvents for all spectroscopic studies. Silica gel column chromatography was performed on Wako gel C-300. Thin-layer chromatography (TLC) was carried out on aluminum sheets coated with silica gel 60 F_{254} (Merck 5554). UV-visible absorption spectra were recorded on a Shimadzu UV-3600. Fluorescence spectra were recorded on a JASCO FP-8500 spectrometer. Absolute fluorescence quantum yields were determined on a HAMAMATSU C9920-02S. Fluorescence lifetime was recorded on a Hamamatsu Photonics Quantaurus-Tau C11367. ^{1}H and ^{13}C NMR spectra were recorded on a JEOL ECA-600 spectrometer (operating as 600 MHz for ^{1}H and 150 MHz for ^{13}C) and chemical shifts were reported as the δ scale in ppm relative to internal standards $CHCl_3$ (δ = 7.26 ppm for ^{1}H, 77.16 ppm for ^{13}C), acetone (δ = 2.05 ppm for ^{1}H, δ = 29.84 ppm for ^{13}C), THF (δ = 25.31 ppm for ^{13}C) and DMSO (δ = 2.50 ppm for ^{1}H). High-resolution atmospheric-pressure-chemical-ionization time-of-flight mass-spectrometry (HR-APCI-TOF-MS) was recorded on a BRUKER micrOTOF model using positive mode. High-resolution matrix-assisted-laser-dissociation-ionization time-of-flight mass spectrometry (HR-MALDI-TOF-MS) was recorded on a BRUKER ultrafleXterme MALDI-TOF/TOF spectrometer using matrix. Single-crystal diffraction analysis data were collected at –180 °C with a Rigaku XtaLAB P200 by using graphite monochromated Cu-$K\alpha$ radiation (λ= 1.54187 Å). The structures were solved by direct methods (SHELXT-2014/5) and refined with full-matrix least squares technique (SHELXT-2014/7)[S3]

2. Experimental Section

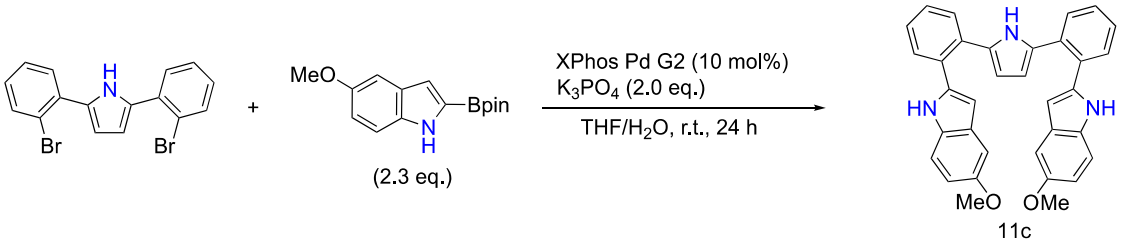

11c

2,5-bis(2-(5-methoxy-1*H*-indol-2-yl)phenyl)-1*H*-pyrrole (11c)

To a 500 mL three-necked round bottom flask, XPhos Pd G2 (472 mg, 0.60 mmol, 10 mol%), 2,5-bis(2-bromophenyl)-1*H*-pyrrole (2.26 g, 6.0 mmol) and 5-methoxy-2-(4,4,5,5-tetramethyl-1,3,2-dioxaborolan-2-yl)-1*H*-indole (3.69 g, 13.5 mmol, 2.3 eq.) were charged. The reaction flask was evacuated and purged with argon three times. After the mixture was dissolved in dry THF (120 mL), degassed aqueous 0.5 M tripotassium phosphate solution (120 mL) was added via syringe and the reaction mixture was stirred at room temperature for 24 h. After quenched with saturated aqueous ammonium chloride solution, the mixture was extracted with ethyl acetate three times and the combined organic layers were washed with water, brine and dried over anhydrous sodium sulfate. After removal of the solvents *in vacuo*, the residue was purified by column chromatography on silica with ethyl acetate/*n*-hexane (*v*/*v* = 1/3) as eluent to give **11c** (2.22 g, yield: 74%) as white solids.

^{1}H NMR (600 MHz, acetone-d_6) δ = 9.96 (s, 2H, NH), 9.38 (s, 1H, NH), 7.50 (dd, J_1 = 7.3, J_2 = 1.4 Hz, 2H, phenylene-H), 7.22–7.28 (m, 8H, phenylene/indole-H), 7.06 (d, J = 2.3 Hz, indole-H), 6.78 (dd, J_1 = 8.7, J_2 = 2.3 Hz, 2H, indole-H), 6.34 (d, J = 2.3 Hz, 2H, pyrrole-H), 5.94 (d, J = 2.8 Hz, 2H, indole-H) and 3.81 (s, 6H, -O-CH_3) ppm

^{13}C NMR (151 MHz, acetone-d_6) δ = 155.22, 139.37, 132.82, 132.75, 132.17, 131.50, 131.44, 130.11, 129.14, 128.91, 127.20, 112.85, 112.73, 110.32, 102.53, 102.34 and 55.85 ppm

HR-APCI-TOF-MS: *m/z* calcd for $C_{34}H_{27}N_3O_2$ M^+: 509.2103; found: 509.2098.

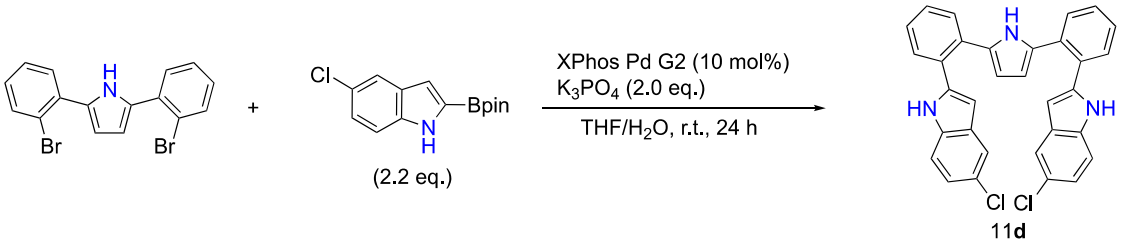

2,5-bis(2-(5-chloro-1*H*-indol-2-yl)phenyl)-1*H*-pyrrole (11d)

To a 300 mL three-necked round bottom flask, XPhos Pd G2 (244 mg, 0.31 mmol, 10 mol%), 2,5-bis(2-bromophenyl)-1*H*-pyrrole (1.17 g, 3.1 mmol) and 5-chloro-2-(4,4,5,5-tetramethyl-1,3,2-dioxaborolan-2-yl)-1*H*-indole (1.89 g, 6.8 mmol, 2.2 eq.) were charged. The reaction flask was evacuated and purged with argon three times. After the mixture was dissolved in dry THF (50 mL), degassed 0.5 M aqueous tripotassium phosphate solution (50 mL) was added via syringe and the reaction mixture was stirred at room temperature for 24 h. After quenched with saturated aqueous ammonium chloride solution, the mixture was extracted with ethyl acetate three times and the combined organic layers were washed with water, brine and dried over anhydrous sodium sulfate. After removal of the solvents *in vacuo*, the residue was purified by column chromatography on silica with dichloromethane/*n*-hexane (*v/v* = 1/1) as eluent to give **11d**. **11d** were used without further purification.

^{1}H NMR (600 MHz, acetone-d_6) δ = 10.31 (s, 2H, NH), 9.55 (s, 1H, NH), 7.51-7.56 (m, 4H, phenylene/indole-H), 7.38 (d, J = 8.7 Hz, 2H, indole-H), 7.26–7.34 (m, 6H, phenylene-H), 7.10 (dd, J_1 = 8.7, J_2 = 1.8 Hz, 2H, indole-H), 6.39 (d, J = 2.3 Hz, 2H, pyrrole-H) and 5.89 (d, J = 2.3 Hz, 2H, indole-H) ppm

^{13}C NMR (151 MHz, acetone-d_6) δ = 140.67, 136.05, 132.95, 132.11, 131.51, 130.99, 130.79, 129.48, 129.25, 127.45, 125.48, 122.39, 120.20, 113.40, 110.52 and 102.13 ppm

HR-APCI-TOF-MS: *m/z* calcd for $C_{32}H_{21}N_3{}^{35}Cl_2$ M^+: 517.1082; found: 517.1107.

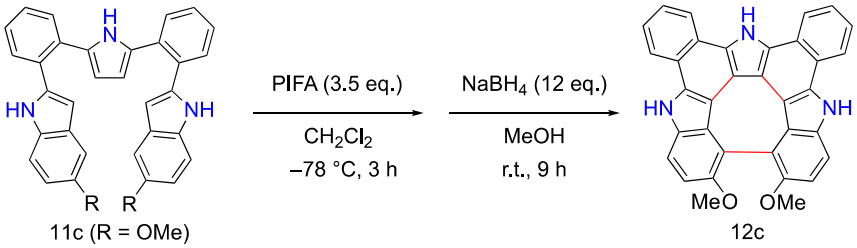

dimethoxy-substituted dibenzotriaza-*quasi*-[8]circulene 12c

To a 300 mL three-necked round bottom flask were charged **11c** (583 mg, 1.1 mmol) and dry dichloromethane (85 mL) under argon, which was cooled to –78 °C. Bis(trifluoroacetoxy)iodobenzene (PIFA, 1.72 g, 4.0 mmol, 3.5 eq.) was then added and the reaction mixture was kept at -78 ˚C for 3 h. Then, the reaction system was allowed to warm to ambient temperature and stirred for 45 min. Next, sodium borohydride (509 mg, 13 mmol, 12 eq.) and methanol (36 mL) were added and the reaction was stirred for 9 h. The mixture was extracted with dichloromethane three times and the combined organic layers were washed with water, brine and dried over anhydrous sodium sulfate. After removal of the solvent *in vacuo*, the residue was purified by recrystallization with dichloromethane/*n*-hexane to afford **12c** (558 mg, yield: 97%) as green solids.

^{1}H NMR (600 MHz, DMSO-d_6) δ = 12.48 (s, 1H, NH), 11.95 (s, 2H, NH), 8.84 (d, J = 8.3 Hz, 2H, phenylene-H), 8.59 (d, J = 8.3 Hz, 2H, phenylene-H), 7.71 (t, J = 7.6 Hz, 2H, phenylene-H), 7.64 (t, J = 7.6 Hz, 2H, phenylene-H), 7.59 (d, J = 8.7 Hz, 2H, indole-H), 7.17 (d, J = 8.7 Hz, 2H, indole-H) and 3.60 (s, 6H, -O-CH_3) ppm.

^{13}C NMR (151 MHz, THF-d_8) δ = 157.37, 138.23, 133.87, 129.04, 125.43, 124.49, 123.11, 123.01, 122.89, 122.49, 122.20, 120.23, 115.67, 115.25, 113.15, 110.90 and 59.02 ppm

HR-APCI-TOF-MS: *m/z* calcd for $C_{34}H_{21}N_3O_2$ M^+: 503.1625; found: 503.1628.

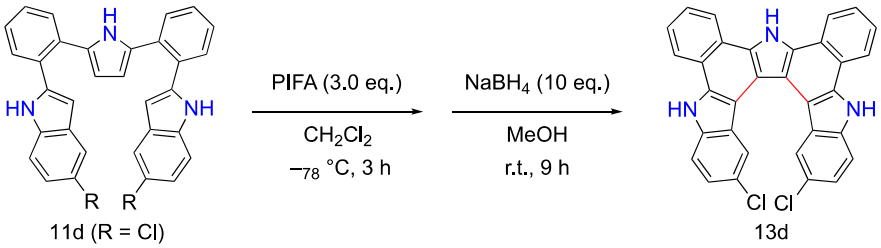

dichloro-substituted dibenzotriaza[7]helicene 13d

To a 200 mL three-necked round bottom flask were charged **11d** (156 mg, 0.30 mmol) and dry dichloromethane (50 mL) under argon, which was cooled to –78 °C. Bis(trifluoroacetoxy)iodobenzene (PIFA, 387 mg, 0.90 mmol, 3.0 eq.) was then added and the reaction mixture was kept at –78 °C for 3 h. Then, the reaction system was allowed to warm to ambient temperature and stirred for 45 min. Next, sodium borohydride (114 mg, 3.0 mmol, 10 eq.) and methanol (10 mL) were added and the reaction was stirred for 9 h. The mixture was extracted with dichloromethane three times and the combined organic layers were washed with water, brine and dried over anhydrous sodium sulfate. After removal of the solvent *in vacuo*, the residue was purified by recrystallization from dichloromethane/*n*-hexane to afford **13d** (147 mg, yield: 95%) as pale yellow solids.

^{1}H NMR (600 MHz, acetone-d_6) δ = 12.03 (s, 1H, NH), 11.50 (s, 2H, NH), 8.84 (d, J = 8.3 Hz, 2H, phenylene-H), 8.65 (d, J = 8.3 Hz, 2H, phenylene-H), 8.10 (d, J = 2.0 Hz, 2H, indole-H), 7.74 (t, J = 7.3 Hz, 2H, phenylene-H), 7.70 (t, J = 7.3 Hz, 2H, phenylene-H), 7.67 (d, J = 8.7 Hz, 2H, indole-H) and 7.30 (dd, J_1 = 8.7Hz, J_2 = 2.0 Hz, 2H, indole-H) ppm.

^{13}C NMR (151 MHz, THF-d_8) δ = 138.37, 134.06, 131.44, 126.26, 126.09, 126.03, 125.23, 124.07, 123.89, 123.13, 122.92, 122.76, 122.03, 114.18, 113.79 and 112.17 ppm.

HR-APCI-TOF-MS: *m/z* calcd for $C_{32}H_{17}N_3{}^{35}Cl_2$ M^+: 513.0784; found: 513.0794.

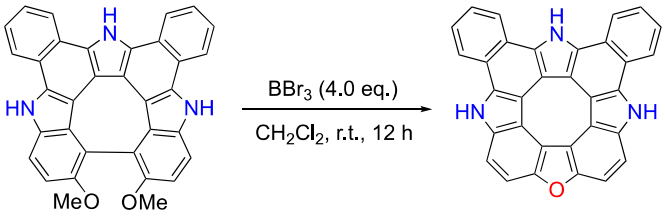

dibenzotriazaoxa[8]circulene 14

To a 1 L four-necked round bottom flask, **12c** (503 mg, 1.0 mmol) was charged. The reaction flask was evacuated and purged with argon three times. After **12c** was dissolved in dry dichloromethane (400 mL), 1.0 M boron tribromide solution in dichloromethane (4.0 mL, 4.0 mmol, 4.0 eq.) was added via syringe and the reaction mixture was stirred at room temperature for 12 h. After quenched with saturated aqueous sodium hydrogen carbonate solution, the mixture was extracted with THF three times and the combined organic layers were washed with water, brine and dried over anhydrous sodium sulfate. After removal of the solvents *in vacuo*, the residue was purified by column chromatography on silica with THF/*n*-hexane (*v*/*v* = 2/1) as eluent to give **14** (331 mg, yield: 73%) as yellow solids.

^{1}H NMR (600 MHz, DMSO-d_6) δ = 12.93 (s, 1H, NH), 12.64 (s, 2H, NH), 9.09 (d, J = 8.3 Hz, 2H, phenylene-H), 8.82 (d, J = 7.8 Hz, 2H, phenylene-H), 7.98 (d, J = 8.7 Hz, 2H, indole-H), 7.96 (d, J = 8.7 Hz, 2H, indole-H) 7.83 (t, J = 7.6 Hz, 2H, phenylene-H) and 7.77 (t, J = 7.6 Hz, 2H, phenylene-H) ppm.

^{13}C NMR (151 MHz, THF-d_8) δ = 152.37, 135.60, 133.26, 130.52, 125.52, 124.92, 123.20, 123.10, 122.11, 116.93, 116.34, 113.46, 112.62, 109.97 and 107.94 ppm.

HR-MALDI-TOF-MS: *m/z* calcd for $C_{32}H_{15}N_3O$ M^+: 457.1210; found: 457.1218.

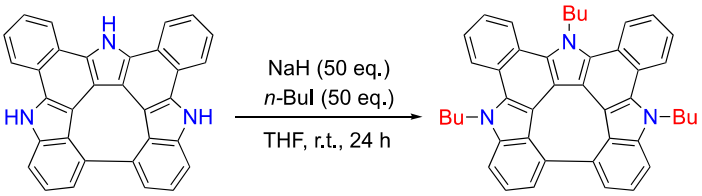

12a 12a-Bu

tri-*N*-butyl-substituted dibenzotriaza-*quasi*-[8]circulene 12a-Bu

To a 30 mL Schlenk tube, **12a** (17.7 mg, 0.040 mmol), sodium hydride (80.0 mg, 60% dispersion in mineral oil, 2.0 mmol, 50 eq.) were charged and the mixture was dissolved in dry THF (50 mL) under argon atmosphere. To this solution was added *n*-iodobutane (0.23 mL, 2.0 mmol, 50 eq.) via syringe and the reaction mixture was stirred at room temperature for 24 h. After quenched with saturated aqueous ammonium chloride solution, the mixture was extracted with ethyl acetate three times and the combined organic layers were washed with water, brine and dried over anhydrous sodium sulfate. After removal of the solvents *in vacuo*, the residue was purified by column chromatography on silica with ethyl acetate/*n*-hexane (*v*/*v* = 1/10) as eluent to give **12a-Bu** (10.5 mg, yield: 43%) as yellow solids.

^{1}H-NMR (600 MHz, DMSO-d_6) δ = 8.72 (d, J = 8.3Hz, 2H, phenylene-H), 8.70 (d, J = 8.3Hz, 2H, phenylene-H), 7.93 (dd, J_1 = 6.9, J_2 = 2.3 Hz, 2H, indole-H), 7.79 (t, J = 7.0 Hz, 2H, phenylene-H), 7.74 (t, J = 7.0 Hz, 2H, phenylene-H), 7.57–7.62 (m, 4H, indole-H), 5.22 (t, J = 7.3 Hz, 2H, N-CH_2-), 4.92 (t, J = 7.8 Hz, 4H, N-CH_2-), 2.05 (m, 4H, -CH$_2$-CH_2-CH$_2$-), 1.53 (tq, J = 14.9 Hz, 4H, -CH$_2$-CH_2-CH$_3$), 1.41–1.46 (m, 2H, -CH$_2$-CH_2-CH$_2$-), 1.00 (t, J = 7.3 Hz, 6H, -CH_3), 0.65–0.70 (tq, J = 14.9, 2H, -CH$_2$-CH_2-CH$_3$) and 0.45 (t, J = 7.3 Hz, 3H, -CH_3) ppm.

^{13}C NMR (151 MHz, $CDCl_3$) δ = 141.70, 136.49, 134.24, 133.34, 127.22, 124.61, 124.02, 123.96, 123.80, 123.71, 123.52, 121.63, 119.71, 117.90, 113.97, 108.85, 52.56, 46.83, 32.53, 31.18, 20.56, 19.94, 14.12 and 13.68 ppm.

HR-APCI-TOF-MS: *m/z* calcd for $C_{44}H_{41}N_3$ M^+: 611.3281; found: 611.3295.

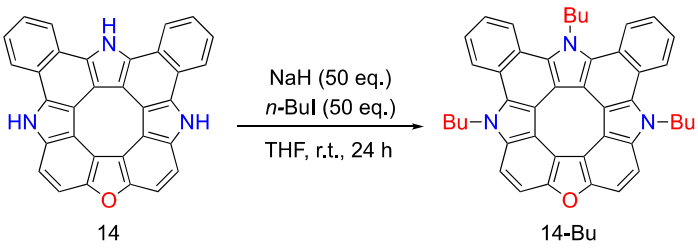

14 14-Bu

tri-*N*-butyl-substituted dibenzotriazaoxa[8]circulene 14-Bu

To a 200 mL three-necked round bottom flask, **14** (45.8 mg, 0.10 mmol), sodium hydride (200 mg, 60% dispersion in mineral oil, 5.0 mmol, 50 eq.) were charged and the mixture was dissolved in dry THF (60 mL) under argon atmosphere. To the mixture was added *n*-iodobutane (0.57 mL, 5.0 mmol, 50 eq.) via syringe and the reaction mixture was stirred at room temperature for 24 h. After quenched with saturated aqueous ammonium chloride solution, the mixture was extracted with ethyl acetate three times and the combined organic layers were washed with water, brine and dried over anhydrous sodium sulfate. After removal of the solvents *in vacuo*, the residue was purified by recrystallization from dichloromethane/*n*-hexane to give **14-Bu** (48.7 mg, yield: 78%) as yellow solids.

^{1}H NMR (600 MHz, $CDCl_3$) δ = 8.80 (d, J = 8.3 Hz, 2H, phenylene-H), 8.74 (d, J = 8.3 Hz, 2H, phenylene-H), 7.86 (d, J = 8.7 Hz, 2H, indole-H), 7.76 (d, J = 8.7 Hz, 2H, indole-H), 7.67–7.73 (m, 4H, phenylene-H), 5.21 (t, J = 7.3 Hz, 2H, N-CH_2-), 5.00 (t, J = 7.8 Hz, 4H, N-CH_2-), 2.23–2.28 (m, 4H, -CH_2-CH_2-CH_2-), 1.67 (tq, J = 14.9 Hz, 4H, -CH_2-CH_2-CH_3), 1.14–1.22 (m, 2H, -CH_2-CH_2-CH_2-), 1.11 (t, J = 7.3 Hz, 6H, -CH_3), 0.67 (tq, J_1 = 14.9 Hz, 2H, -CH_2-CH_2-CH_3) and 0.39 (t, J = 7.3 Hz, 3H, -CH_3) ppm.

^{13}C NMR (151 MHz, $CDCl_3$) δ = 151.39, 137.45, 136.45, 132.56, 124.79, 124.21, 124.10, 123.88, 123.17, 121.94, 117.29, 116.10, 114.39, 112.86, 107.85, 107.47, 54.31, 46.84, 32.48, 30.61, 20.55, 19.94, 14.12 and 13.51 ppm.

HR-APCI-TOF-MS: *m/z* calcd for $C_{44}H_{39}N_3O$ M^+: 625.3070; found: 625.3088.

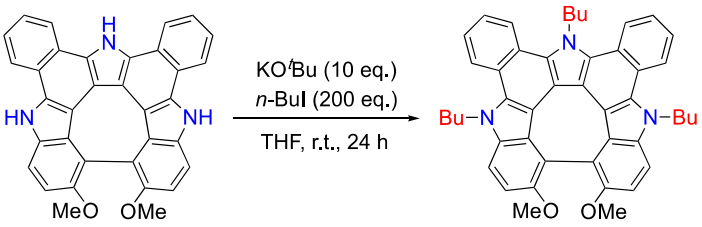

12c 12c-Bu

tri-*N*-butyl-dimethoxy-substituted dibenzotriaza-*quasi*-[8]circulene 12c-Bu

To a 200 mL three-necked round bottom flask, **12c** (50.3 mg, 0.10 mmol) was charged and dissolved in dry THF (60 mL) under argon atmosphere. To the mixture was added *n*-iodobutane (2.3 mL, 20 mmol, 200 eq.) and 1 M potassium *tert*-butoxide in THF (1.0 mL, 1.0 mmol, 10 eq.) via syringe and the reaction mixture was stirred at room temperature for 24 h. After quenched with saturated aqueous ammonium chloride solution, the mixture was extracted with ethyl acetate three times and the combined organic layers were washed with water, brine and dried over anhydrous sodium sulfate. After removal of the solvents *in vacuo*, the residue was purified by column chromatography on silica with ethyl acetate/*n*-hexane (*v*/*v* = 1/4) as eluent to give **12c-Bu** (30.7 mg, yield: 46%) as yellow solids.

^{1}H NMR (600 MHz, DMSO-d_6) δ = 8.64 (t, J = 9.2 Hz, 4H, phenylene-H), 7.69–7.76 (m, 6H, phenylene/indole-H), 7.25 (d, J = 8.7 Hz, 2H, indole-H), 5.22 (m, 1H, N-CH_2-), 5.10 (m, 1H, N-CH_2-), 4.73–4.84 (m, 4H, N-CH_2-), 1.93–2.02 (m, 4H, -CH$_2$-CH_2-CH$_2$-), 1.43–1.62 (m, 6H, -CH$_2$-CH_2-CH$_2$-/-CH$_2$-CH_2-CH$_3$), 0.98 (t, J = 7.3 Hz, 6H, -CH_3), 0.79 (tq, J = 14.9 Hz, 2H, -CH$_2$-CH_2-CH$_3$) and 0.53 (t, J = 7.3 Hz, 3H, -CH_3) ppm.

^{13}C NMR (151 MHz, CDCl$_3$) δ = 156.01, 138.38, 134.32, 132.81, 124.56, 124.02, 123.79, 123.60, 121.93, 121.18, 119.41, 117.77, 114.70, 112.87, 108.84, 59.28, 51.67, 46.86, 32.74, 31.37, 20.59, 19.97, 14.13 and 13.75 ppm.

HR-APCI-TOF-MS: *m/z* calcd for $C_{46}H_{45}N_3O_2$ M^+: 671.3497; found: 671.3506.

3. NMR Spectra

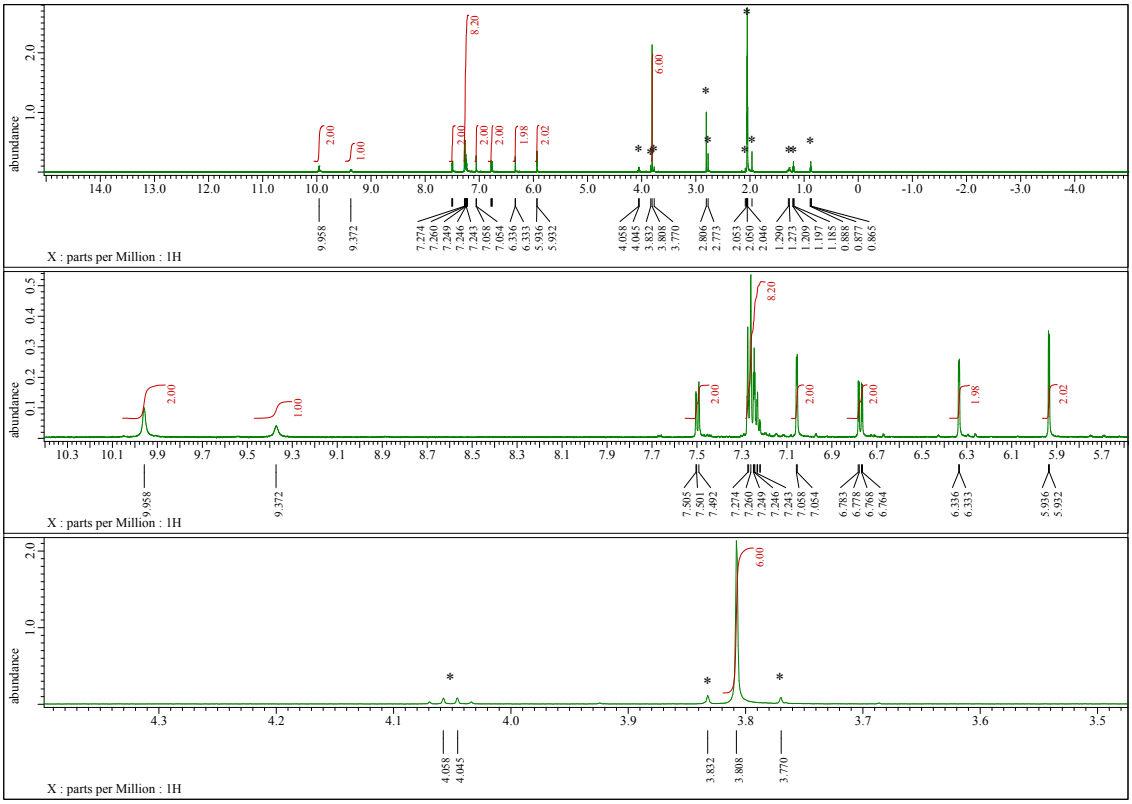

Figure S3-1. ^{1}H NMR spectrum of **11c** in acetone-d_6 at room temperature. Peaks with * are due to residual solvents and impurities.

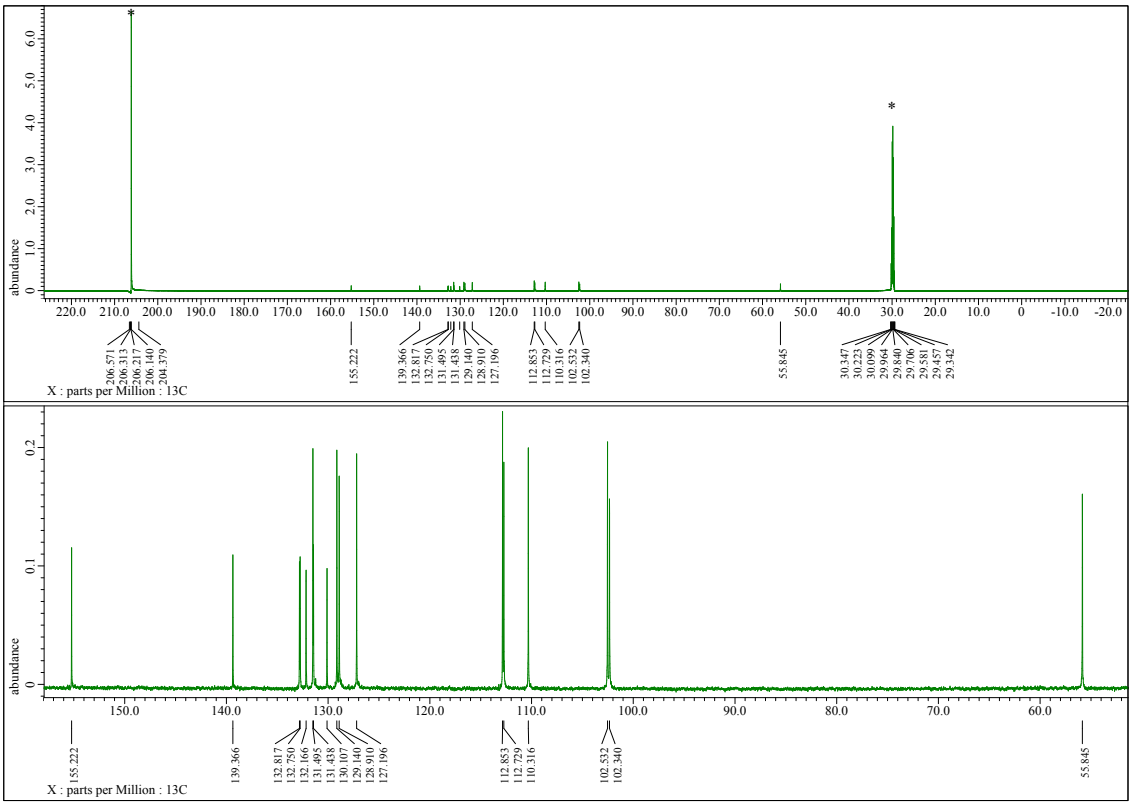

Figure S3-2. ^{13}C NMR spectrum of **11c** in acetone-d_6 at room temperature. Peaks with * are due to residual solvent.

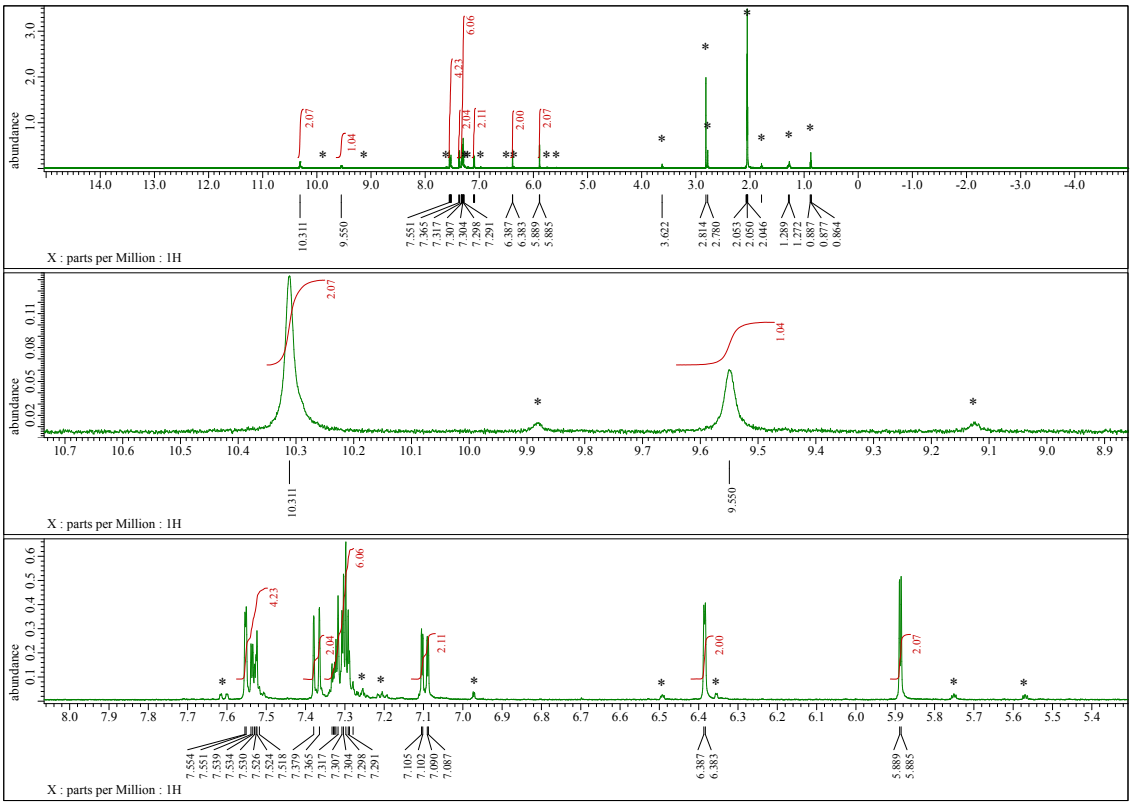

Figure S3-3. ^{1}H NMR spectrum of **11d** in acetone-d_6 at room temperature. Peaks with * are due to residual solvents and impurities.

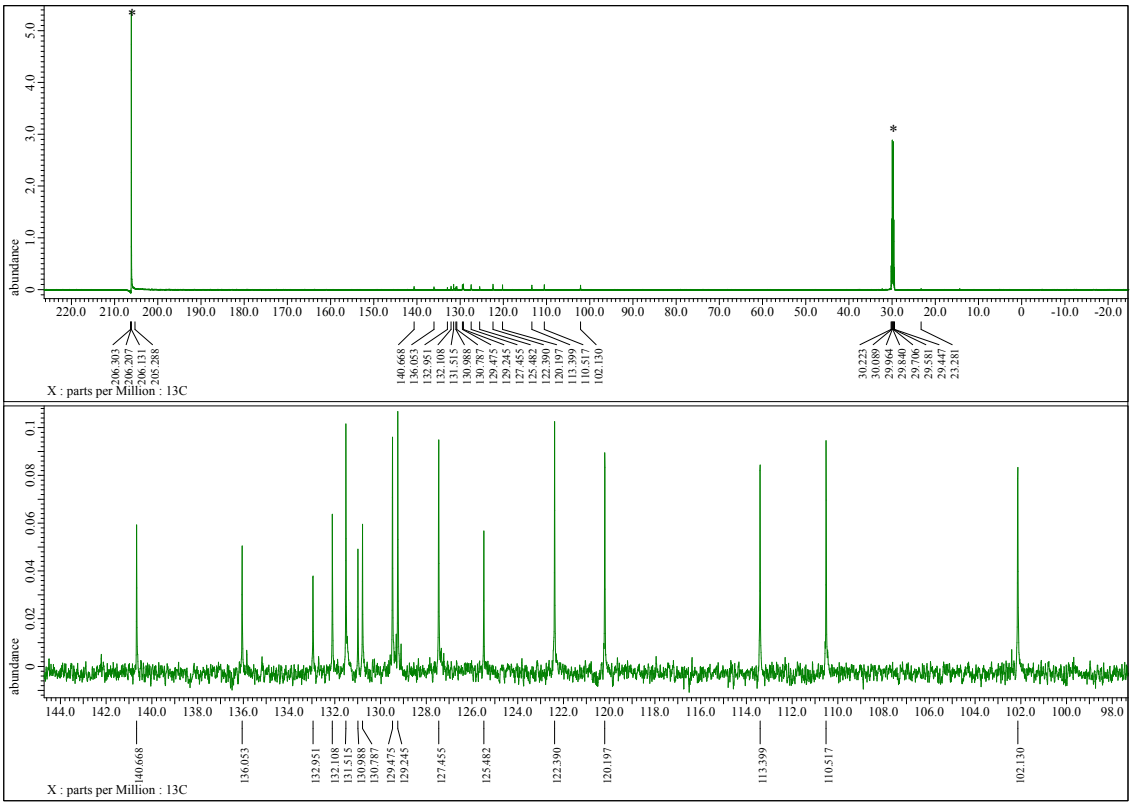

Figure S3-4. ^{13}C NMR spectrum of **11d** in acetone-d_6 at room temperature. Peaks with * are due to residual solvent.

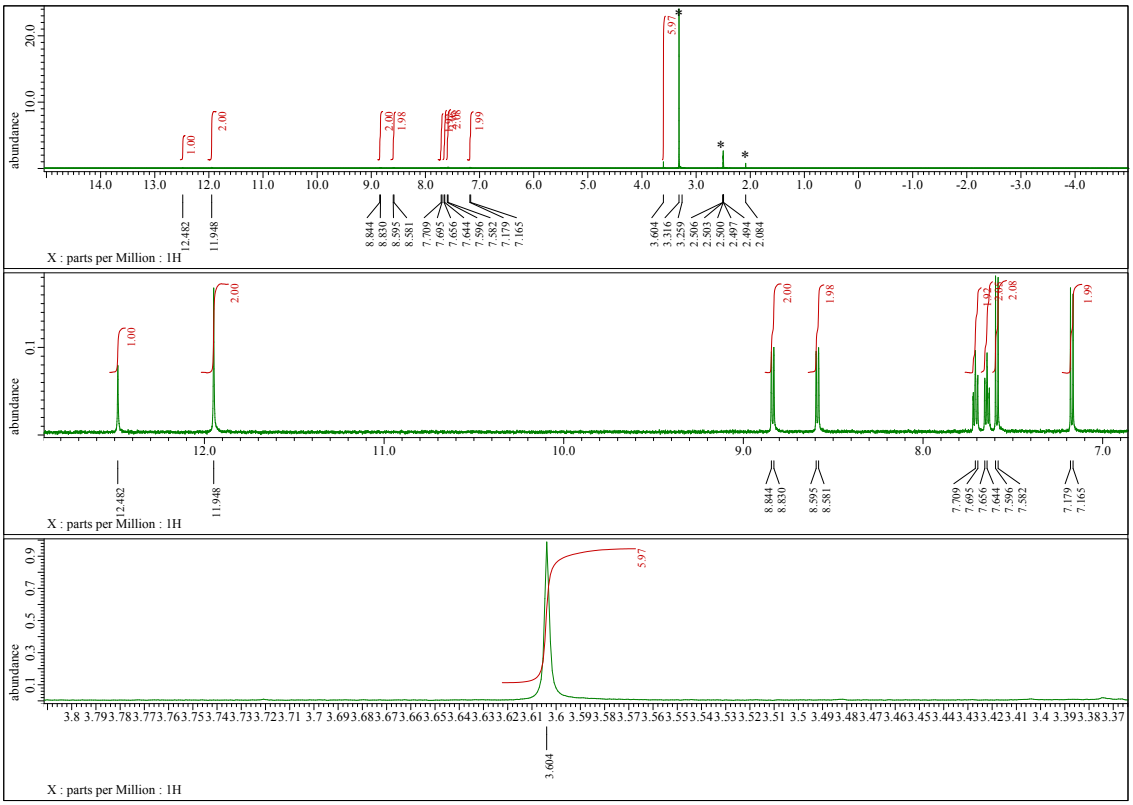

Figure S3-5. ^{1}H NMR spectrum of **12c** in DMSO-d_6 at room temperature. Peaks with * are due to residual solvents and impurities.

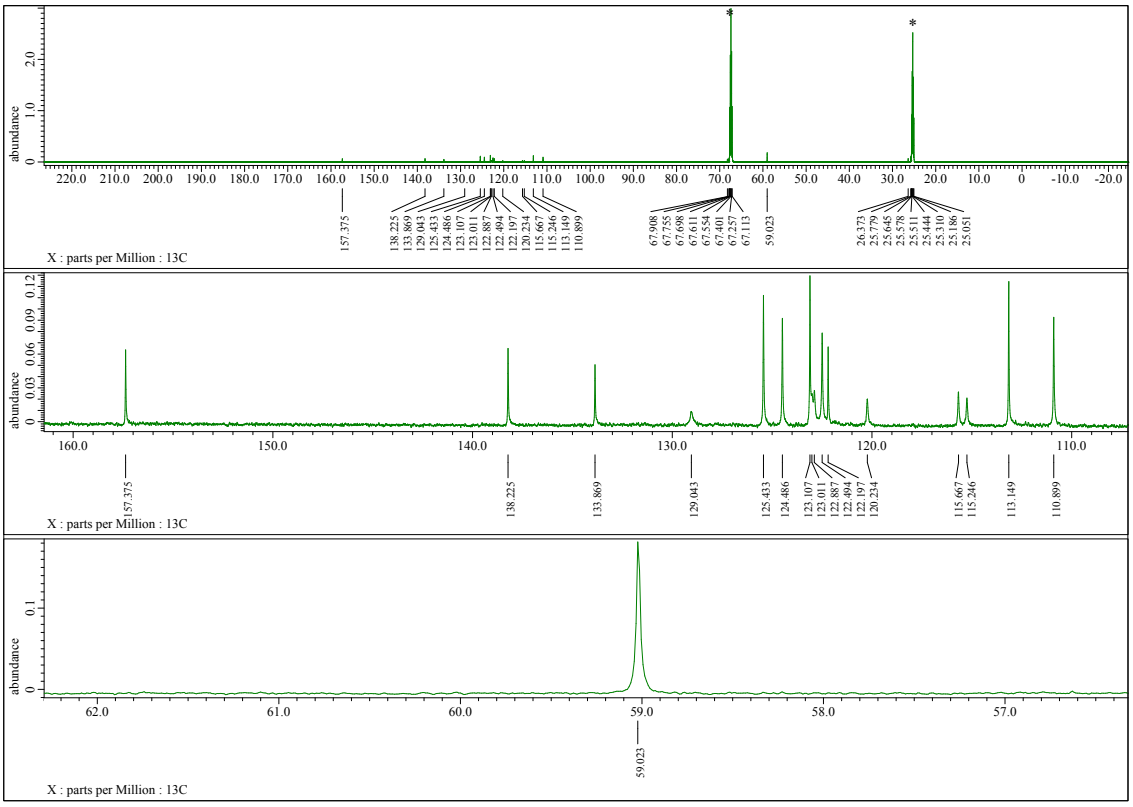

Figure S3-6. ^{13}C NMR spectrum of **12c** in THF-d_8 at room temperature. Peaks with * are due to residual solvent.

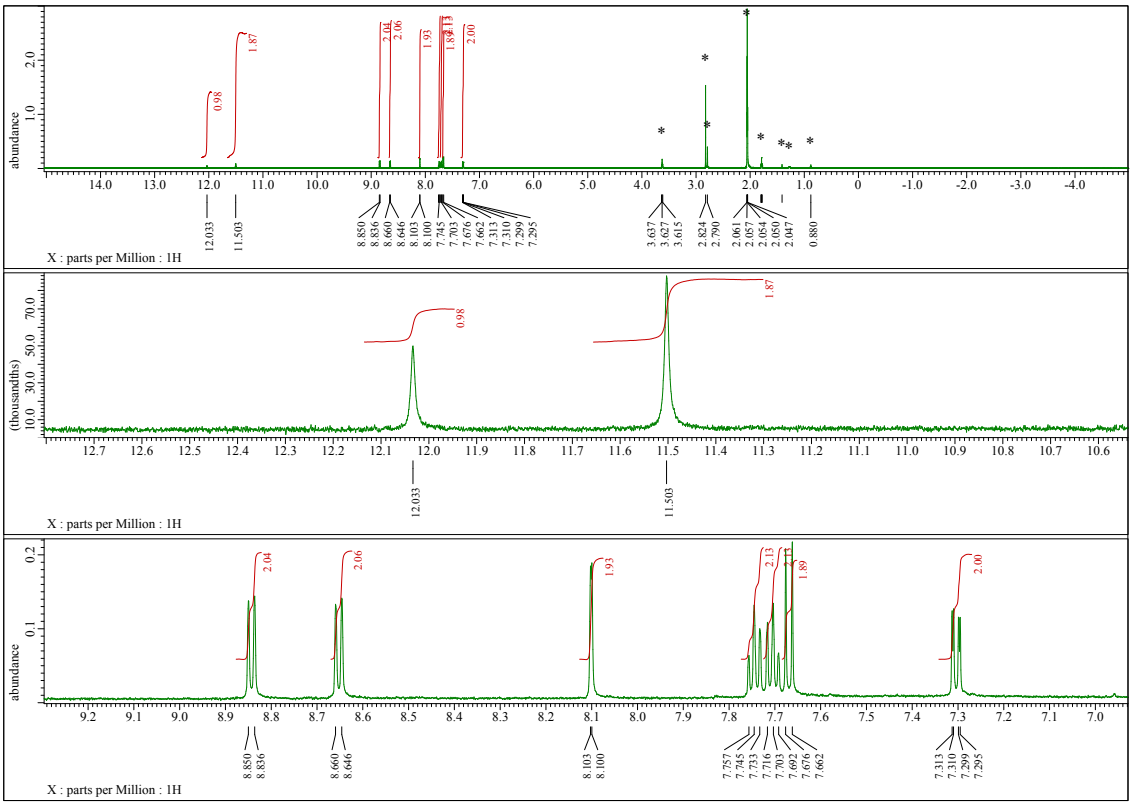

Figure S3-7. ^{1}H NMR spectra of **13d** in acetone-d_6 at room temperatures. Peaks with * are due to residual solvents and impurities.

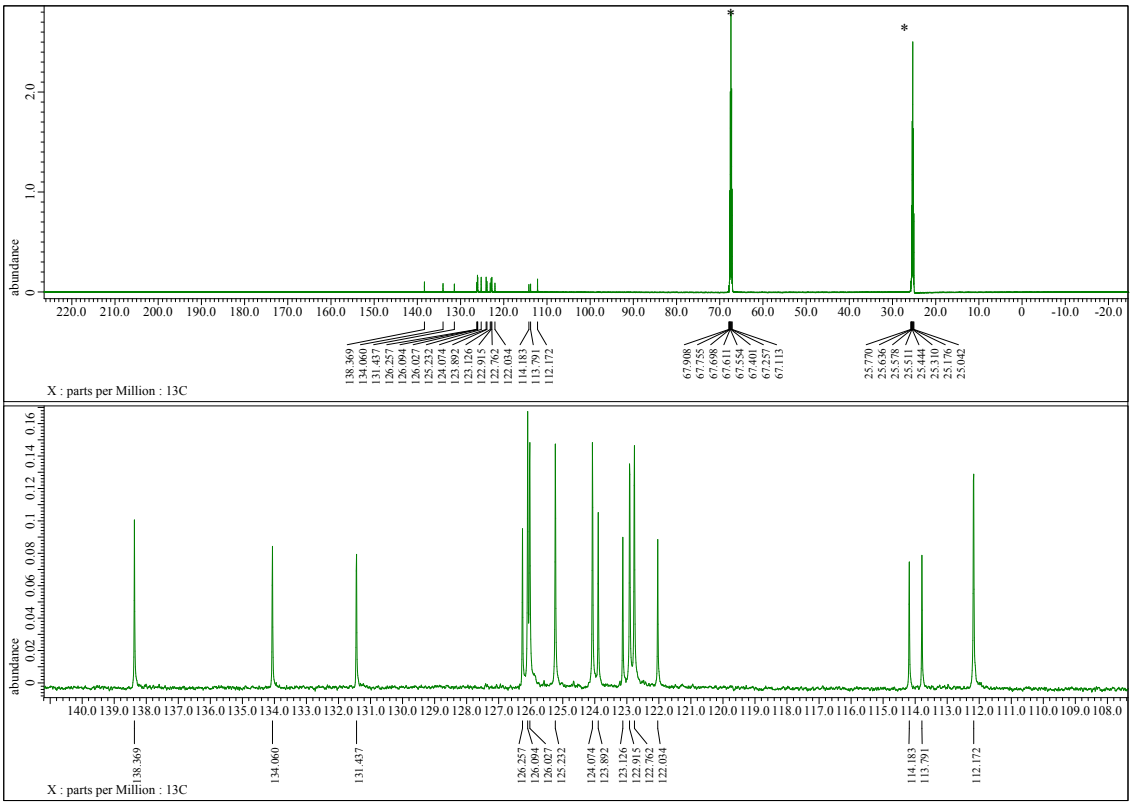

Figure S3-8. ^{13}C NMR spectrum of **13d** inTHF-d_8 at room temperature. Peaks with * are due to residual solvents.

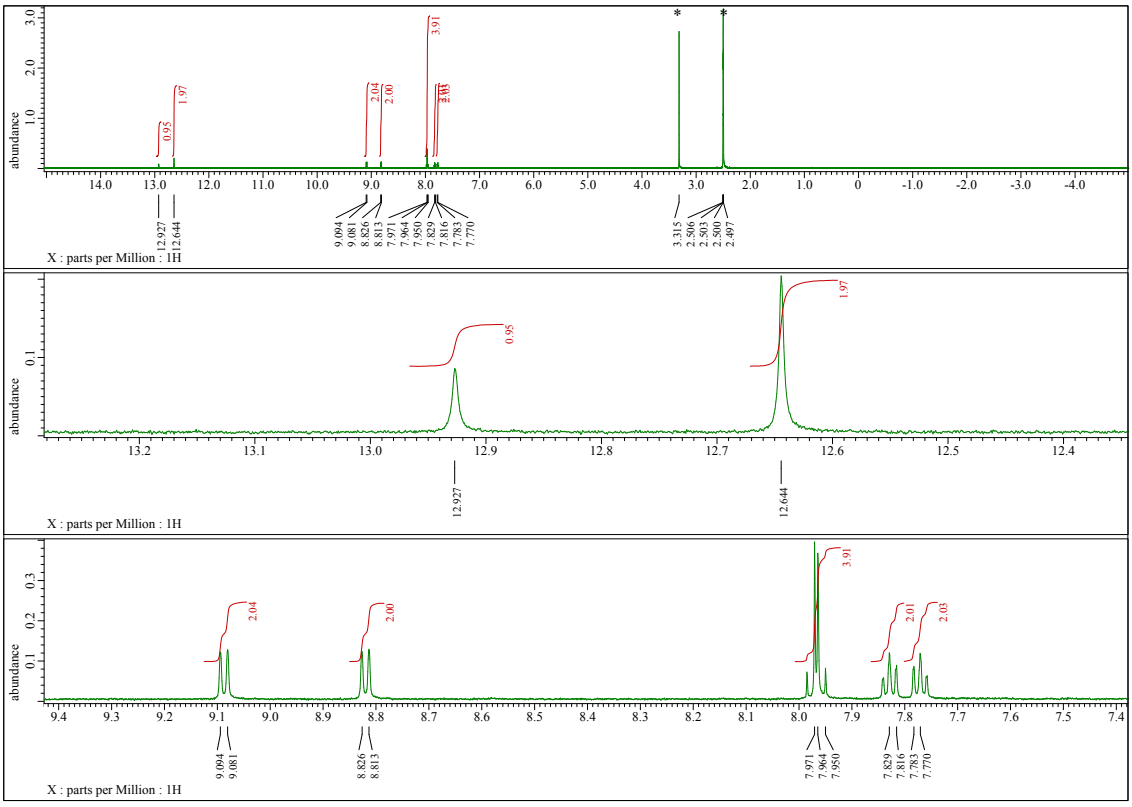

Figure S3-9. ^{1}H NMR spectrum of **14** in DMSO-d_6 at room temperature. Peaks with * are due to residual solvents.

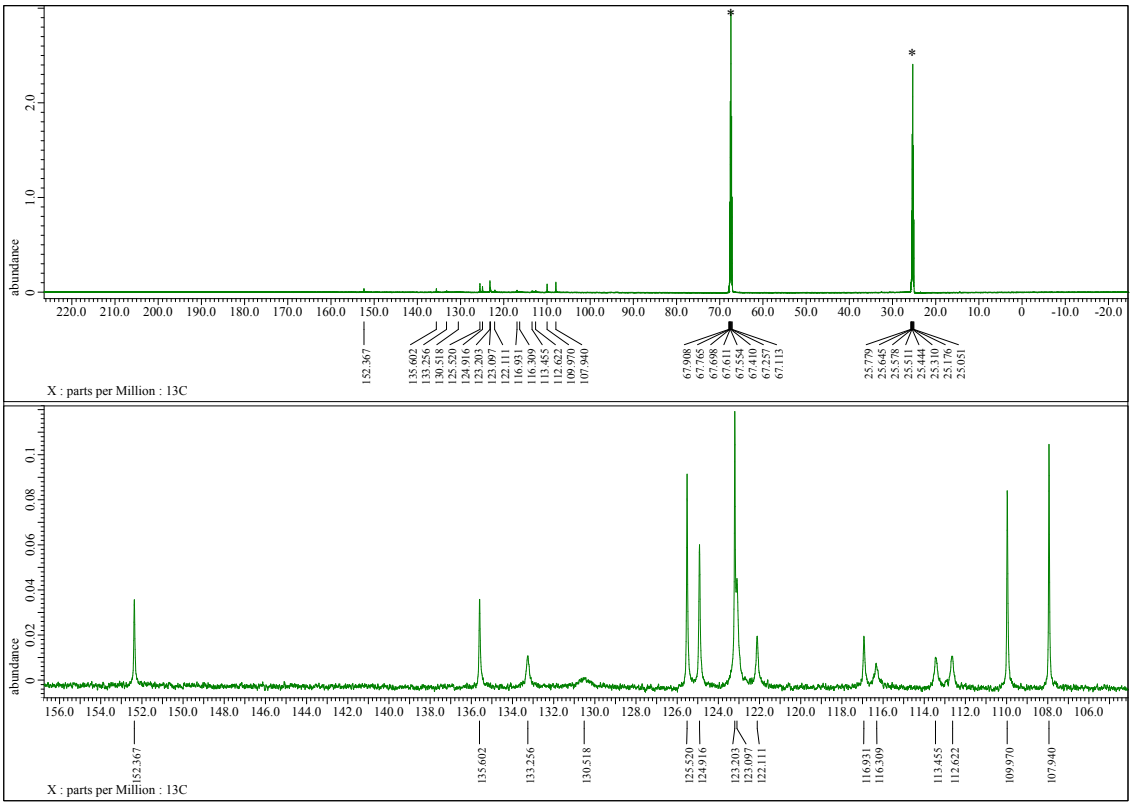

Figure S3-10. ^{13}C NMR spectra of **14** in THF-d_8 at room temperatures. Peaks with * are due to residual solvents.

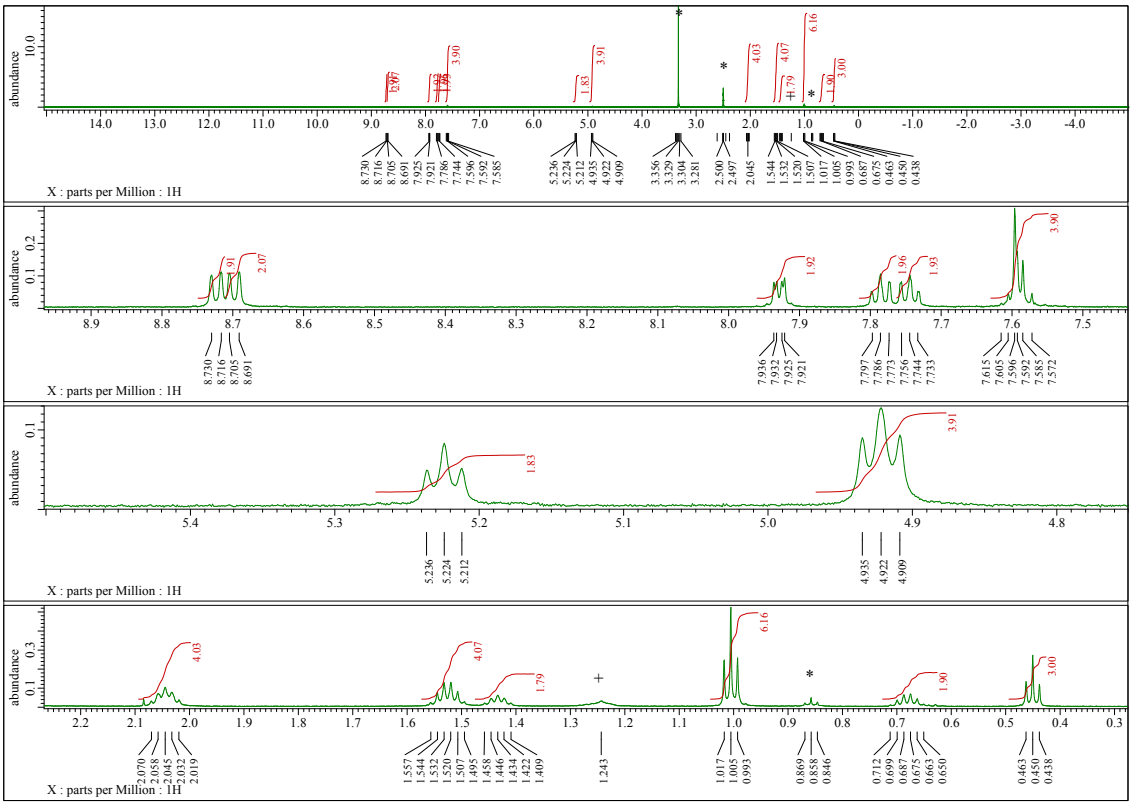

Figure S3-11. ^{1}H NMR spectrum of **12a-Bu** in DMSO-d_6 at room temperature. Peaks with * are due to residual solvents and impurities.

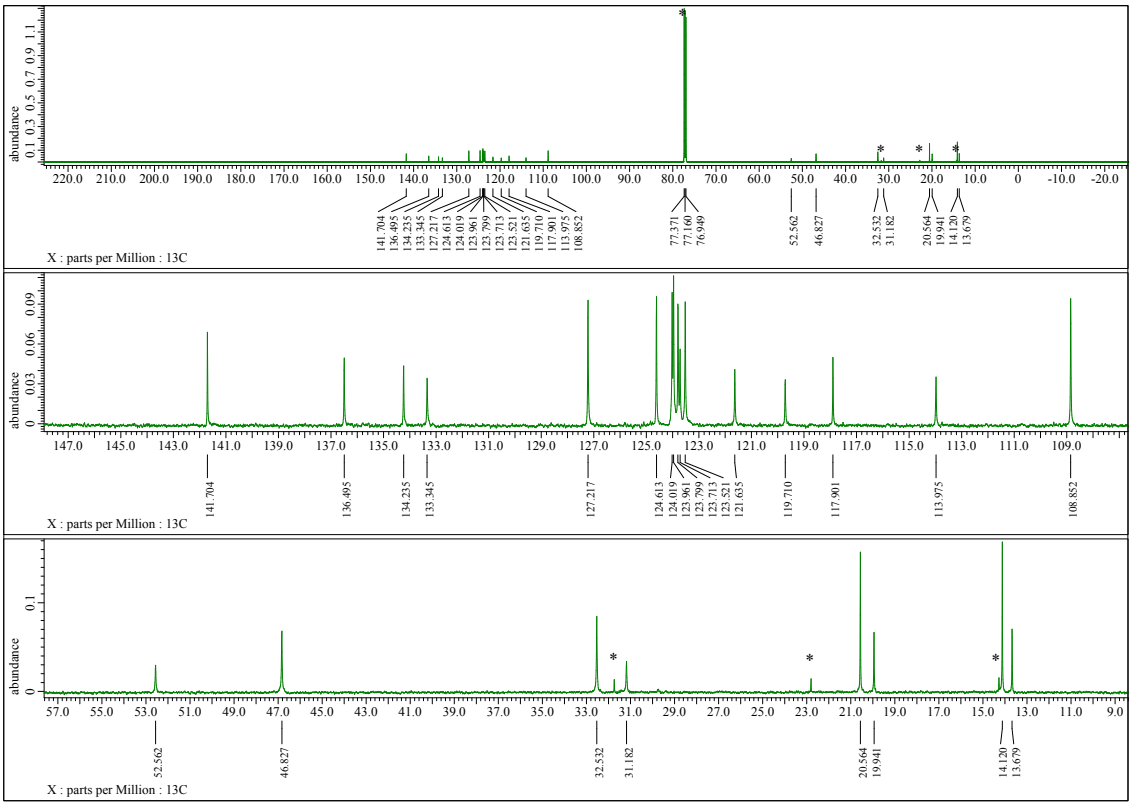

Figure S3-12. ^{13}C NMR spectrum of **12a-Bu** in $CDCl_3$ at room temperature. Peaks with * are due to residual solvents.

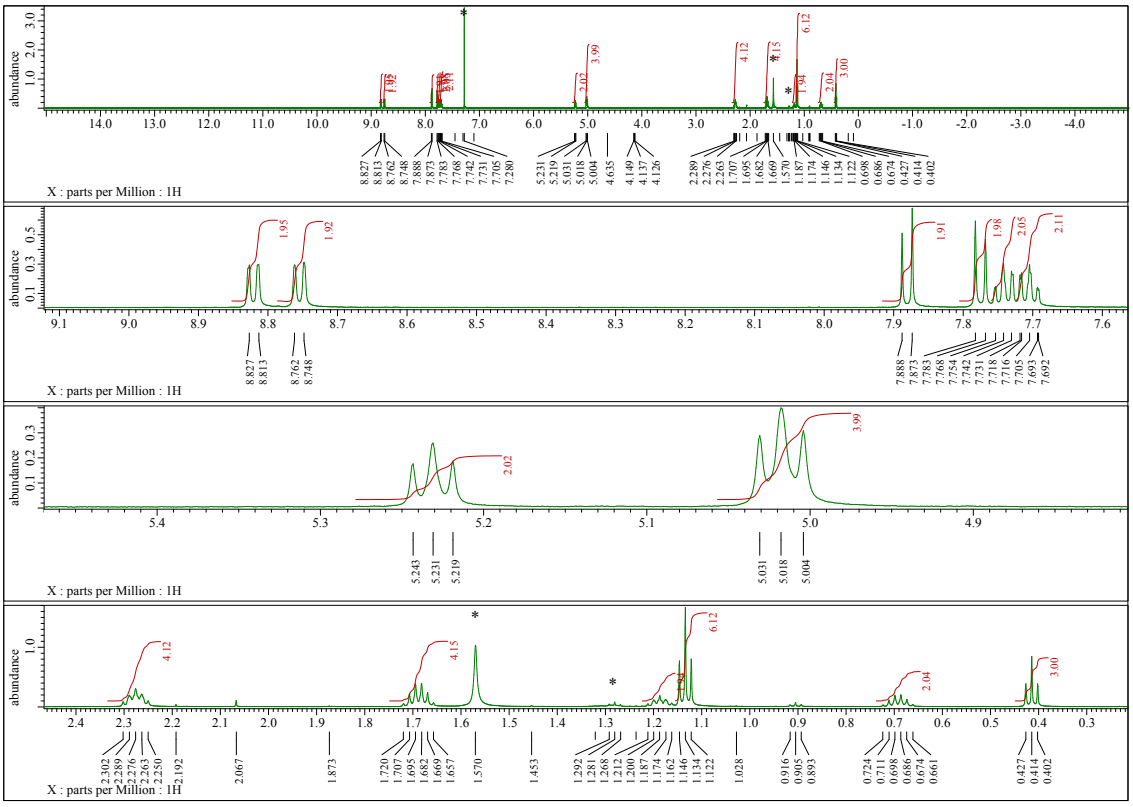

Figure S3-13. ^{1}H NMR spectrum of **14-Bu** in $CDCl_3$ at room temperature. Peaks with * are due to residual solvents and impurities.

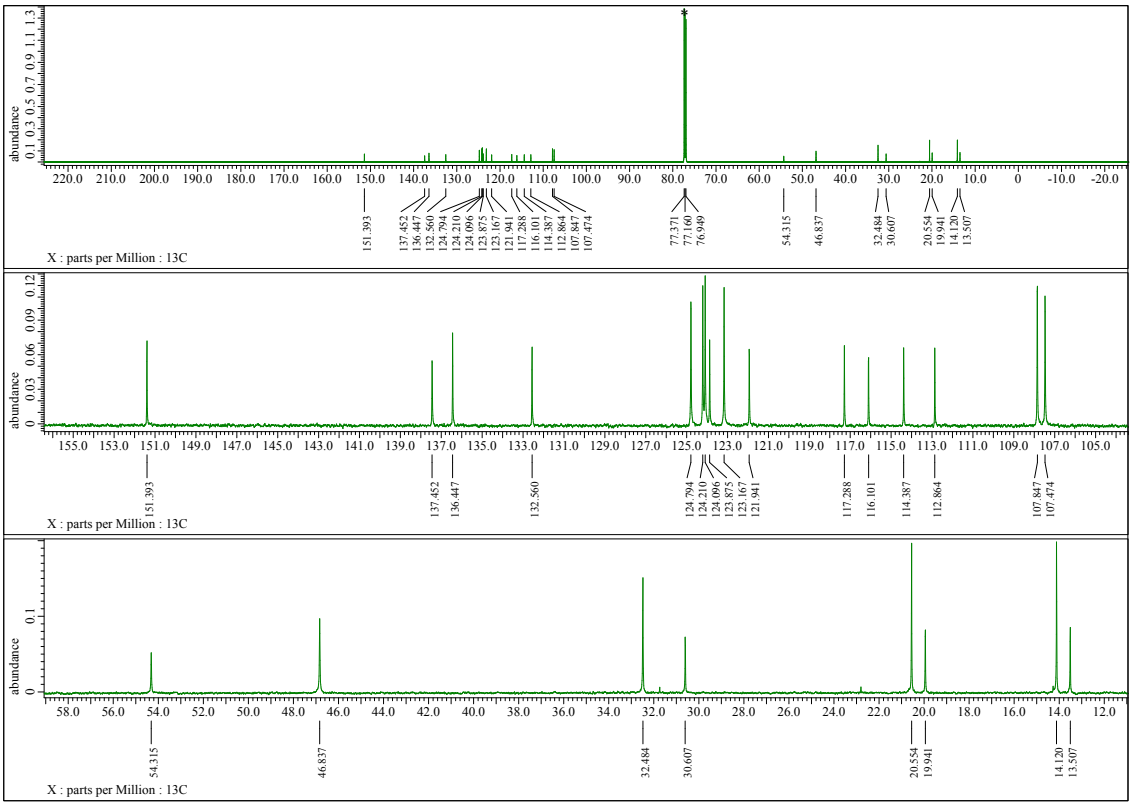

Figure S3-14. ^{13}C NMR spectra of **14-Bu** in $CDCl_3$ at room temperature. Peak with * are due to residual solvent.

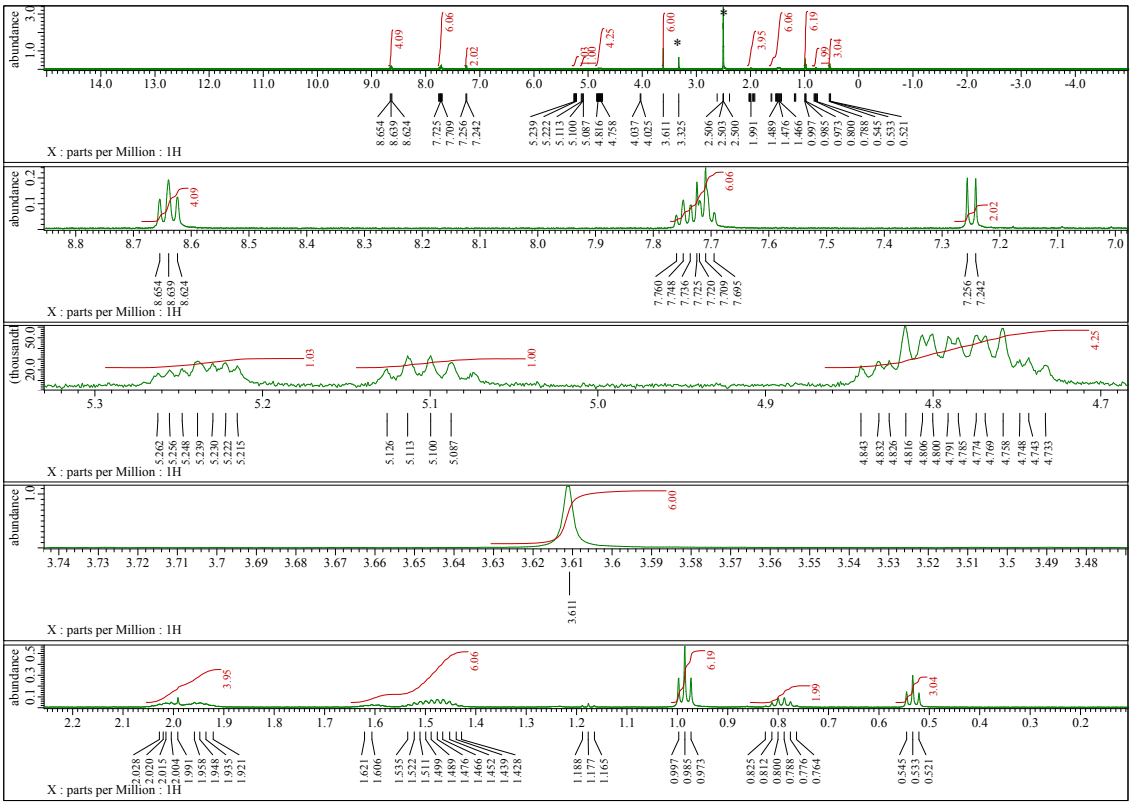

Figure S3-15. ^{1}H NMR spectrum of **12c-Bu** in DMSO-d_6 at room temperature. Peaks with * are due to residual solvents and impurities.

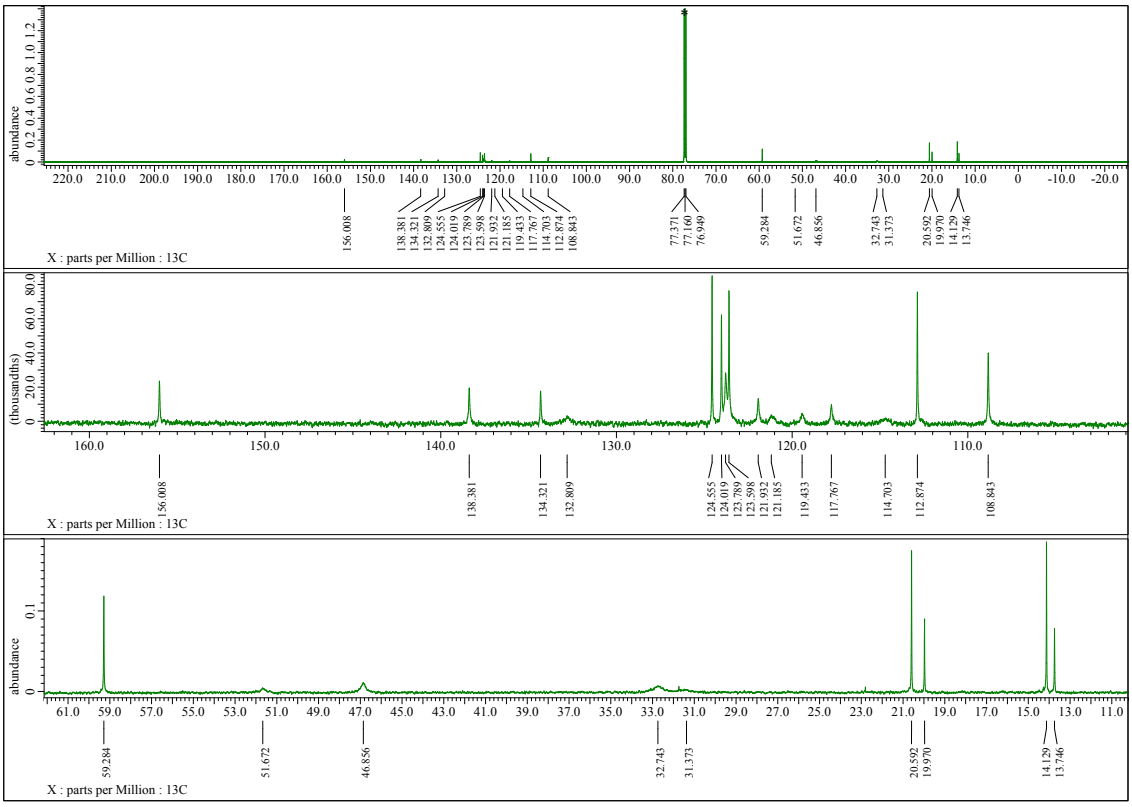

Figure S3-16. ^{13}C NMR spectrum of **12c-Bu** in $CDCl_3$ at room temperature. Peak with * are due to residual solvent.

4. Mass Spectra

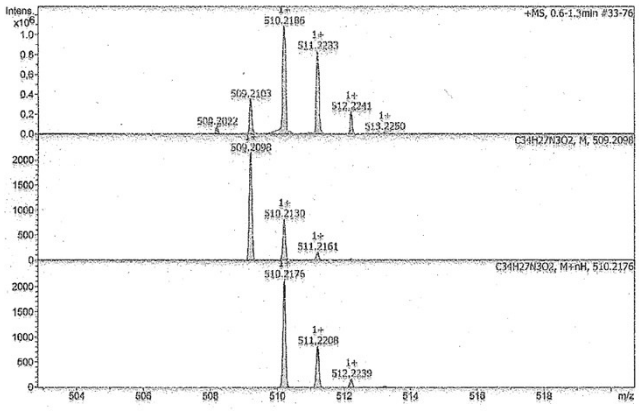

Figure S4-1. APCI-TOF-mass spectra of **11c** (Top; observed. Bottom; calculated).

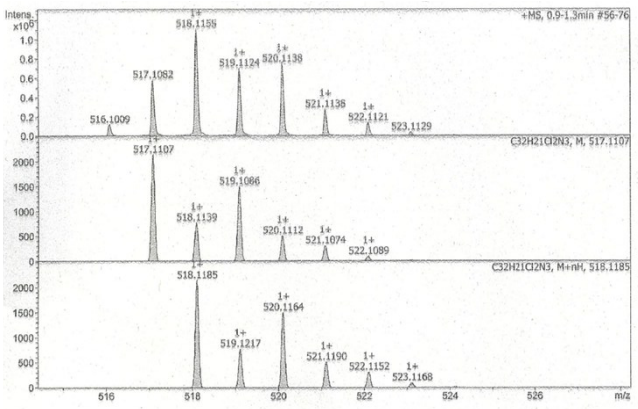

Figure S4-2. APCI-TOF-mass spectra of **11d** (Top; observed. Bottom; calculated).

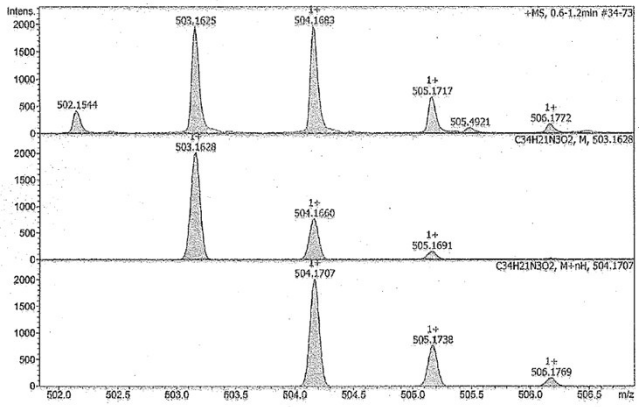

Figure S4-3. APCI-TOF-mass spectra of **12c** (Top; observed. Bottom; calculated).

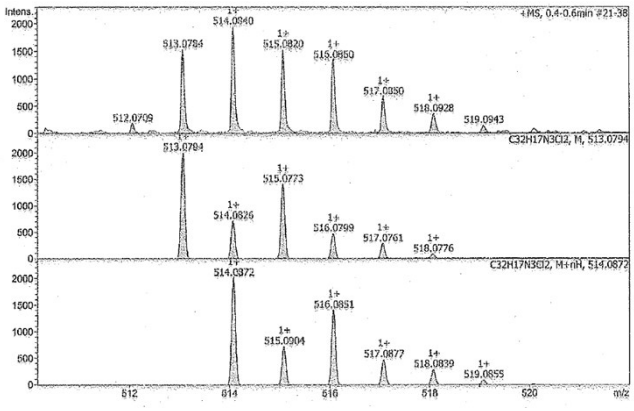

Figure S4-4. APCI-TOF-mass spectra of **13d** (Top; observed. Middle; simulated as $[M]^+$, Bottom; simulated as $[M+H]^+$).

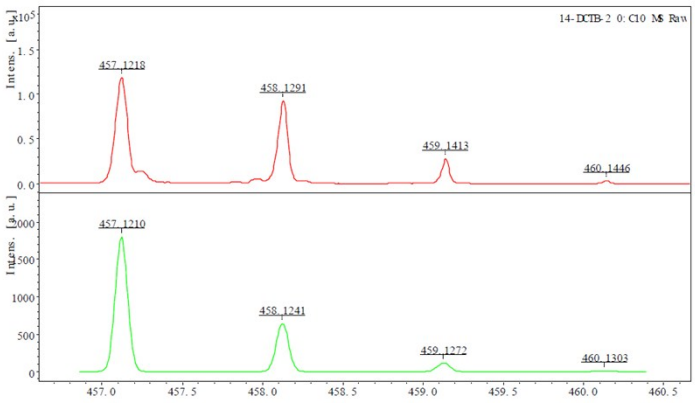

Figure S4-5. HR-MALDI-TOF-mass spectra of **14** (Top; observed. Bottom; simulated).

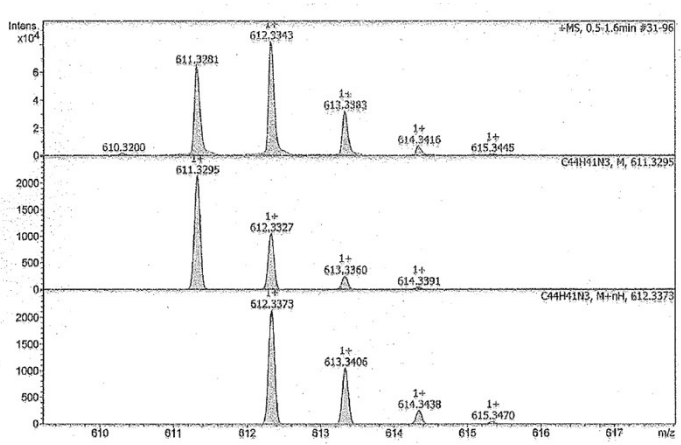

Figure S4-6. APCI-TOF-mass spectra of **12a-Bu** (Top; observed. Middle; simulated as $[M]^+$, Bottom; simulated as $[M+H]^+$).

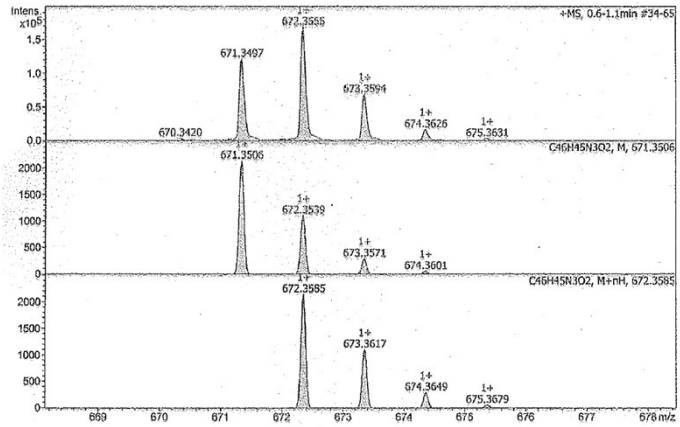

Figure S4-7. APCI-TOF-mass spectra of **12c-Bu** (Top; observed. Middle; simulated as $[M]^+$, Bottom; simulated as $[M+H]^+$).

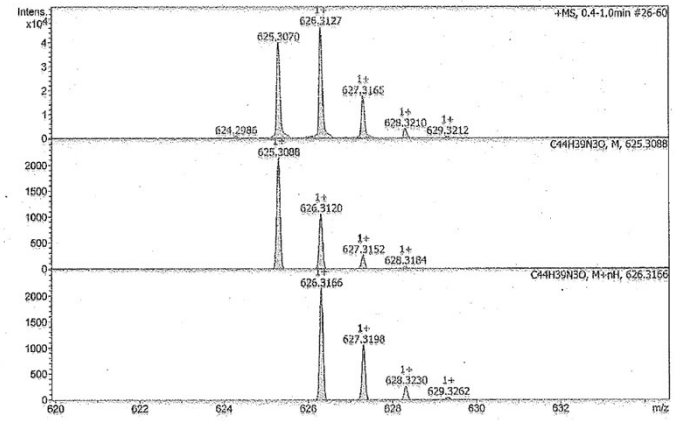

Figure S4-8. APCI-TOF-mass spectra of **14-Bu** (Top; observed. Middle; simulated as $[M]^+$, Bottom; simulated as $[M+H]^+$).

*For **11c**, **11d**, **12c**, **13d**, **12a-Bu**, **12c-Bu** and **14-Bu**, the observed mass peaks were likely considered to be a mixture of [M] and [M+H].

5. DFT Calculations

All calculations were carried out using the Gaussian 16 program. All structures were fully optimized without any symmetry restriction. The calculations were performed by the density functional theory (DFT) method with restricted B3LYP level[S5], employing a basis set 6-311G(d,p) for all atoms. Spin density distributions have been calculated at the UB3LYP/6-311G(d,p) level. NICS[S6] values have been obtained with the GIAO method at the B3LYP/6-311G(d,p) level. Excitation energies and oscillator strengths were calculated with the TD-SCF method at the B3LYP level.

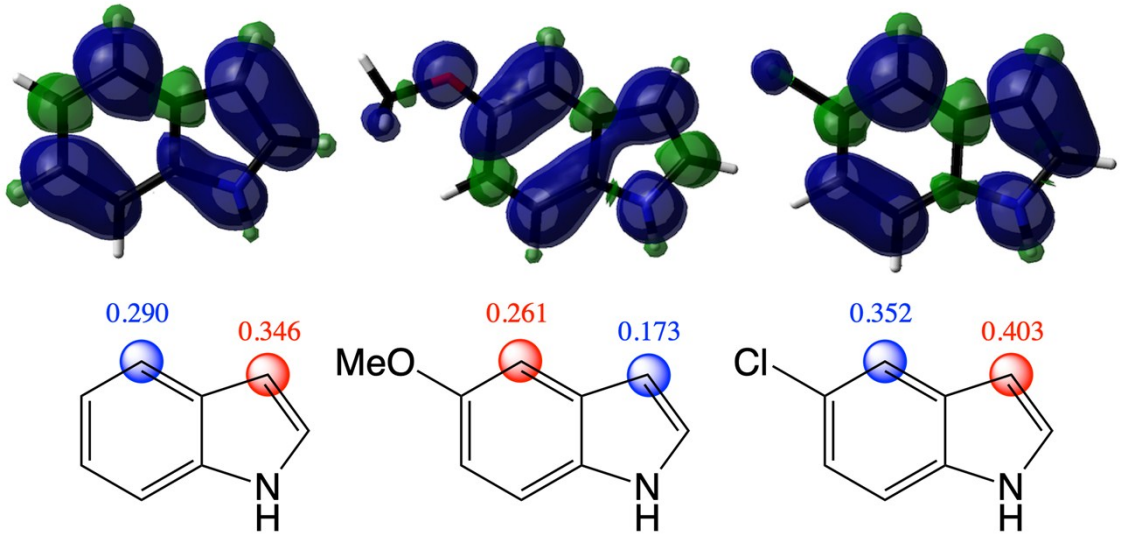

Figure 5-1. Spin density distribution of the radical cations of 1*H*-indole, 5-methoxy-1*H*-indole and 5-chloro-1*H*-indole calculated at the UB3LYP/6-311G(d,p) level.

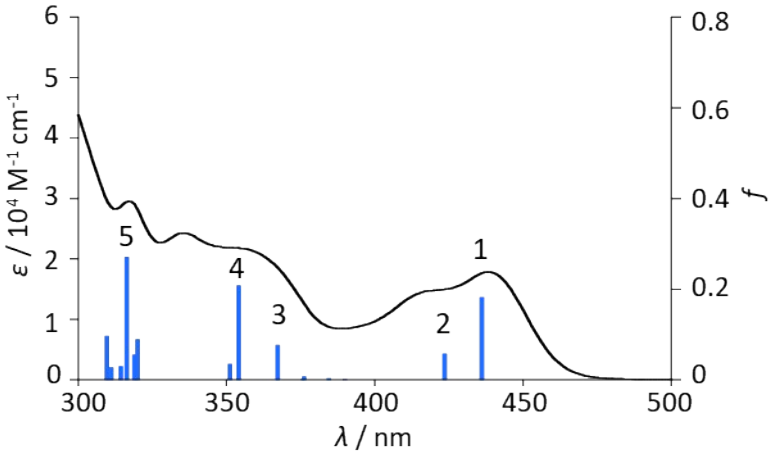

Figure S5-2. Experimental molar absorption in THF and calculated oscillator strengths *f* on the basis of optimized structure of **12c**.

Table S5-1. Selected calculated electronic transition of **12c** at the B3LYP/6-311G(d,p) level.

No.	Wavelength (nm)	coefficients	Electronic Transition	*f*
1	436.13	0.69255	131 HOMO → 132 LUMO	0.1816
2	423.65	-0.12399 0.68703	129 HOMO-2 → 134 LUMO+2 130 HOMO-1 → 132 LUMO	0.0568
3	376.15	0.12335 0.53834 0.42423	128 HOMO-3 → 132 LUMO 130 HOMO-1 → 133 LUMO+1 131 HOMO → 134 LUMO+2	0.0065
4	354.13	0.67397 -0.13094	128 HOMO-3 → 132 LUMO 131 HOMO → 134 LUMO+2	0.2073
5	316.44	-0.16005 -0.40783 0.52152 -0.10859	127 HOMO-4 → 132 LUMO 128 HOMO-3 → 134 LUMO+2 129 HOMO-2 → 133 LUMO+1 131 HOMO → 135 LUMO+3	0.2708

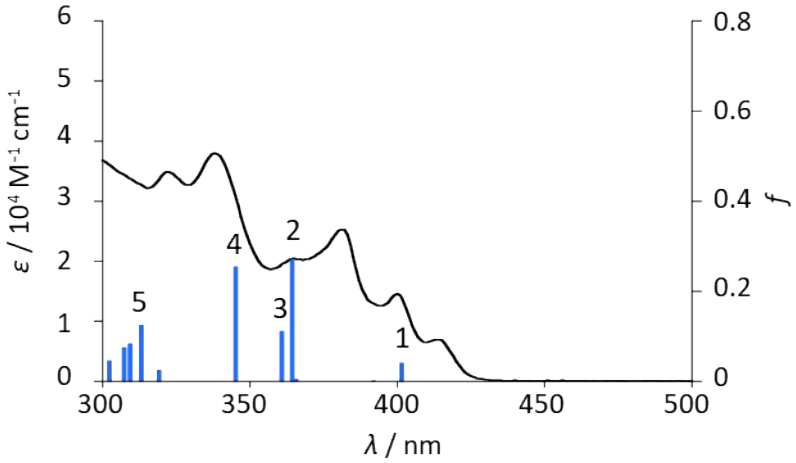

Figure S5-3. Experimental molar absorption in THF and calculated oscillator strengths *f* on the basis of optimized structure of **13d**.

Table S5-2. Selected calculated electronic transition of **13d** at the B3LYP/6-311G(d,p) level.

No.	Wavelength (nm)	coefficients	Electronic Transition	*f*
1	401.50	0.24013 0.64850	131 HOMO-1 → 134 LUMO+1 132 HOMO → 133 LUMO	0.0400
2	364.30	0.46514 0.40778 0.27637	131 HOMO-1 → 133 LUMO 131 HOMO-1 → 135 LUMO+2 132 HOMO → 134 LUMO+1	0.2690
3	360.88	-0.10383 0.63871 -0.24467 -0.10674	129 HOMO-3 → 133 LUMO 131 HOMO-1 → 134 LUMO+1 132 HOMO → 133 LUMO 132 HOMO → 135 LUMO+2	0.1113
4	345.28	-0.20350 -0.31823 0.53392 -0.23005	130 HOMO-2 → 133 LUMO 131 HOMO-1 → 133 LUMO 131 HOMO-1 → 135 LUMO+2 132 HOMO → 134 LUMO+1	0.2541
5	313.20	0.66192 0.10754 0.13145	129 HOMO-3 → 133 LUMO+1 130 HOMO-2 → 134 LUMO+2 131 HOMO-1 → 136 LUMO+4	0.1244

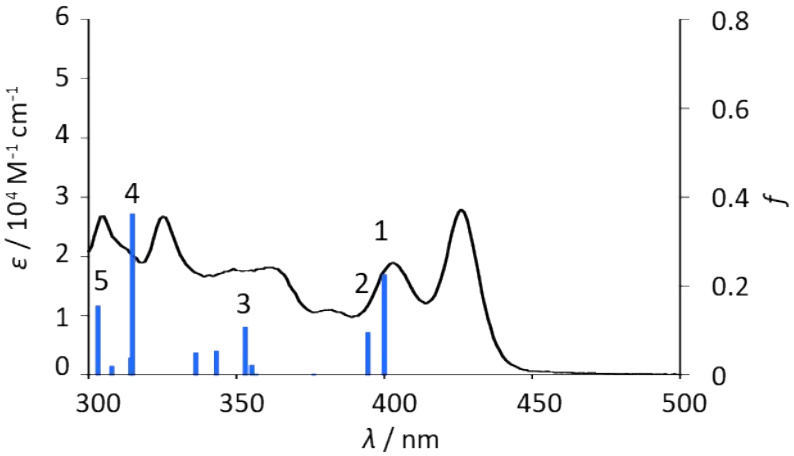

Figure S5-4. Experimental molar absorption in THF and calculated oscillator strengths *f* on the basis of optimized structure of **14**.

Table S5-3. Selected calculated electronic transition of **14** at the B3LYP/6-311G(d,p) level.

No.	Wavelength (nm)	coefficients	Electronic Transition	*f*
1	399.95	0.13880 0.67662	116 HOMO-2 → 120 LUMO+1 118 HOMO → 119 LUMO	0.2254
2	394.49	0.15531 -0.14463 0.66334	115 HOMO-3 → 119 LUMO 116 HOMO-2 → 121 LUMO+2 117 HOMO-1 → 119 LUMO	0.0948
3	352.92	0.51982 -0.15151 0.42562	115 HOMO-3 → 119 LUMO 117 HOMO-1 → 119 LUMO 117 HOMO-1 → 120 LUMO+1	0.1079
4	314.83	0.44027 0.37606 -0.15875 -0.13933	114 HOMO-4 → 119 LUMO 116 HOMO-2 → 120 LUMO+1 117 HOMO-1 → 121 LUMO+2 118 HOMO → 119 LUMO	0.3625
5	303.17	0.63011 0.10550 0.13167 0.22115	116 HOMO-2 →121 LUMO+2 117 HOMO-1 → 119 LUMO 117 HOMO-1 → 120 LUMO+1 118 HOMO → 123 LUMO+4	0.1552

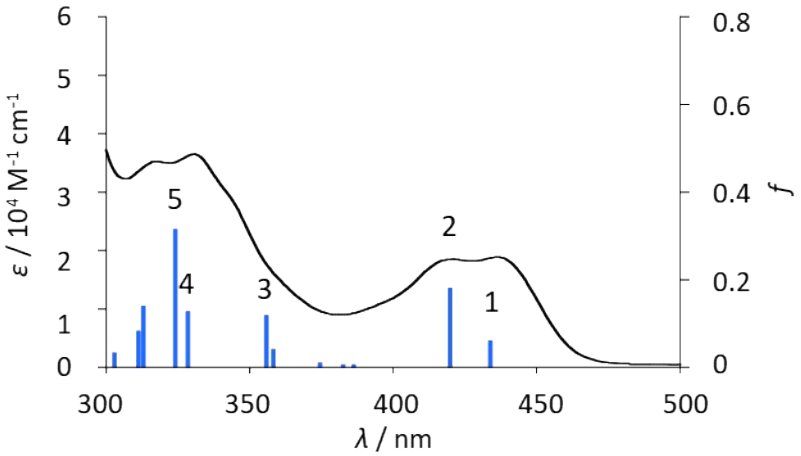

Figure S5-5. Experimental molar absorption in THF and calculated oscillator strengths *f* on the basis of optimized structure of **12a-Bu**.

Table S5-4. Selected calculated electronic transition of **12a-Bu** at the B3LYP/6-311G(d,p) level

No.	Wavelength (nm)	coefficients	Electronic Transition	*f*
1	433.95	-0.10001 -0.11995 0.68025	161 HOMO-2 → 166 LUMO+2 162 HOMO-1 → 164 LUMO 163 HOMO → 164 LUMO	0.0609
2	419.96	0.11086 0.67303 0.11775	161 HOMO-2 → 165 LUMO+1 162 HOMO-1 → 164 LUMO 163 HOMO → 164 LUMO	0.1809
3	355.91	-0.13304 -0.17105 -0.38329 0.39344 -0.16764 -0.32267	161 HOMO-2 → 164 LUMO 161 HOMO-2 → 165 LUMO+1 162 HOMO-1 → 165 LUMO+1 162 HOMO-1 → 166 LUMO+2 163 HOMO → 165 LUMO+1 163 HOMO → 166 LUMO+2	0.1184
4	328.58	0.66942	160 HOMO-3 → 164 LUMO	0.1280
5	324.14	-0.35689 0.55804 -0.10654 0.11546	159 HOMO-4 → 164 LUMO 161 HOMO-2 → 165 LUMO +1 162 HOMO-1 → 164 LUMO 162 HOMO-1 → 167 LUMO+3	0.3150

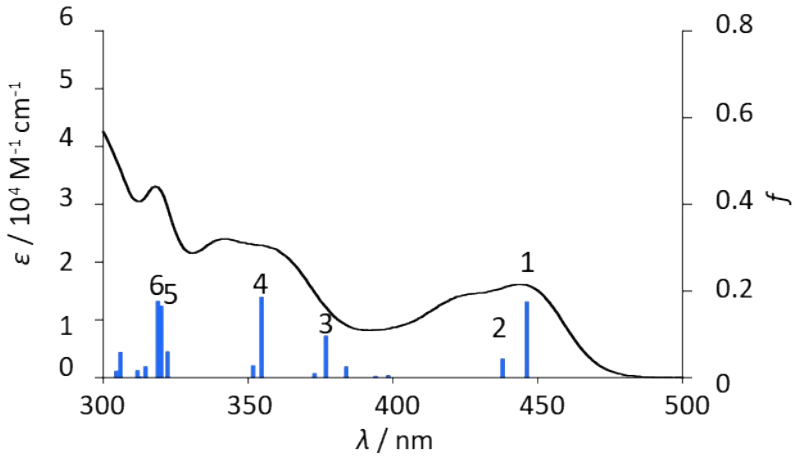

Figure S5-6. Experimental molar absorption in THF and calculated oscillator strengths *f* on the basis of optimized structure of **12c-Bu**.

Table S5-5. Selected calculated electronic transition of **12c-Bu** at the B3LYP/6-311G(d,p) level.

No.	Wavelength (nm)	coefficients	Electronic Transition	*f*
1	446.27	0.69201	179 HOMO → 180 LUMO	0.1752
2	437.86	0.68999	178 HOMO-1 → 180 LUMO	0.0446
3	376.98	0.13631	175 HOMO-4 → 180 LUMO	0.0961
		-0.18227	176 HOMO-3 → 180 LUMO	
		-0.18689	177 HOMO-2 → 180 LUMO	
		0.58211	178 HOMO-1 → 182 LUMO+2	
		-0.21770	179 HOMO → 181 LUMO+1	
4	354.66	0.56271	176 HOMO-3 → 180 LUMO	0.1866
		-0.37071	177 HOMO-2 → 180 LUMO	
		0.12156	179 HOMO → 182 LUMO+2	
5	319.99	-0.15847	175 HOMO-4 → 180 LUMO	0.1653
		0.46270	175 HOMO-4 → 181 LUMO+1	
		-0.19140	176 HOMO-3 → 181 LUMO+1	
		0.14011	176 HOMO-3 → 182 LUMO+2	
		-0.23150	177 HOMO-2 → 181 LUMO+1	
		-0.13631	177 HOMO-2 → 182 LUMO+2	
		-0.13801	178 HOMO-1 → 184 LUMO+4	
		0.27852	179 HOMO → 183 LUMO-3	
6	318.90	0.10102	175 HOMO-4 → 180 LUMO	0.1765
		0.20709	175 HOMO-4 → 181 LUMO+1	
		0.25925	176 HOMO-3 → 181 LUMO+1	
		0.25977	176 HOMO-3 → 182 LUMO+2	
		0.41917	177 HOMO-2 → 181 LUMO+1	
		-0.33440	177 HOMO-2 → 182 LUMO+2	

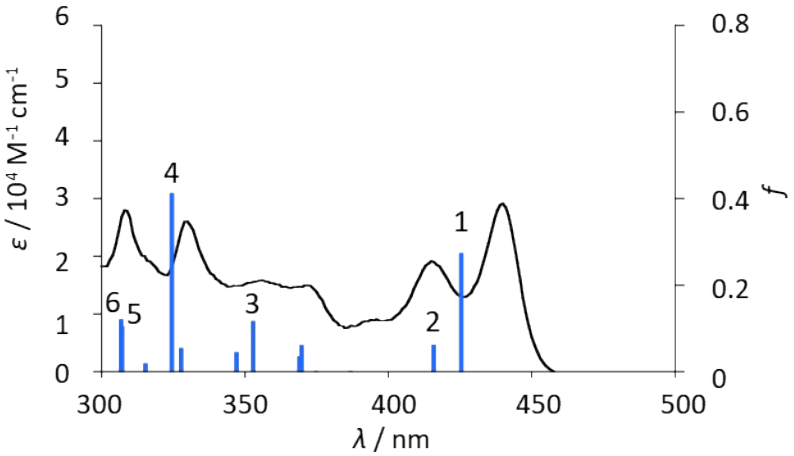

Figure S5-7. Experimental molar absorption in THF and calculated oscillator strengths *f* on the basis of optimized structure of **14-Bu**.

Table S5-6. Selected calculated electronic transition of **14-Bu** at the B3LYP/6-311G(d,p) level.

No.	Wavelength (nm)	coefficients	Electronic Transition	*f*
1	425.48	0.12707	163 HOMO-3 → 168 LUMO+1	0.2737
		0.68436	166 HOMO → 167 LUMO	
2	415.82	-0.12348	163 HOMO-3 → 169 LUMO+2	0.0618
		0.11279	164 HOMO-2 → 167 LUMO	
		0.67768	165 HOMO-1 → 167 LUMO	
3	352.92	0.24859	164 HOMO-2 → 167 LUMO	0.1160
		-0.19788	165 HOMO-1 → 168 LUMO+1	
		0.60739	166 HOMO → 169 LUMO+2	
4	324.57	-0.36808	162 HOMO-4 → 167 LUMO	0.4116
		0.54462	163 HOMO-3 → 168 LUMO+1	
		-0.15857	165 HOMO-1 → 168 LUMO+2	
		-0.12765	166 HOMO → 167 LUMO	
5	307.25	-0.27859	162 HOMO-4 → 167 LUMO	0.1047
		-0.13033	163 HOMO-3 → 168 LUMO+1	
		0.44751	163 HOMO-3 → 169 LUMO+2	
		-0.29277	164 HOMO-2 → 169 LUMO+2	
		-0.10217	166 HOMO → 170 LUMO+3	
		0.24710	166 HOMO → 171 LUMO+4	
6	306.84	0.30522	162 HOMO-4 → 167 LUMO	0.1198
		0.14147	163 HOMO-3 → 168 LUMO+1	
		0.41992	163 HOMO-3 → 169 LUMO+2	
		0.29102	164 HOMO-2 → 169 LUMO+2	
		0.10963	165 HOMO-1 → 170 LUMO+3	
		-0.25922	166 HOMO → 170 LUMO+3	

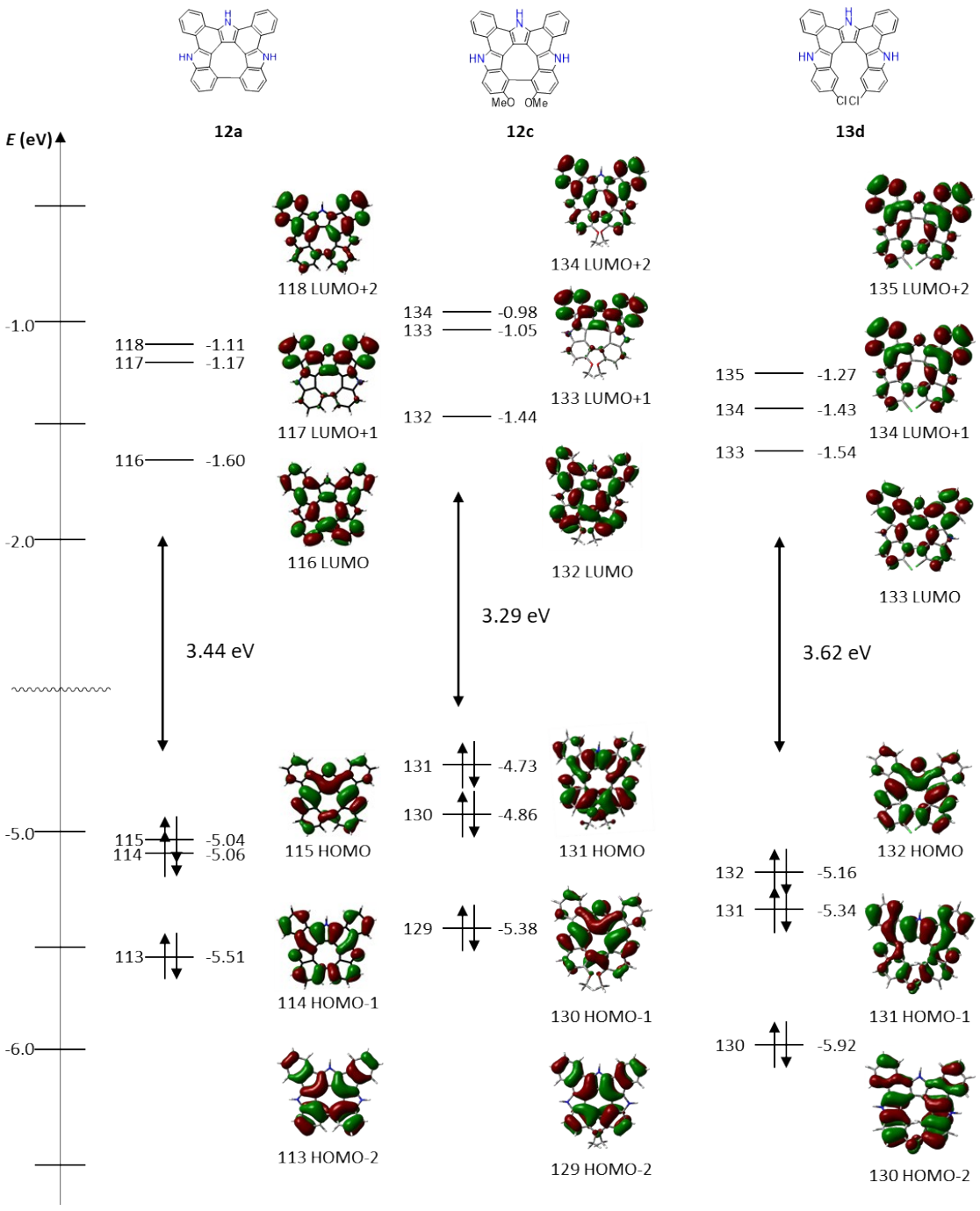

Figure S5-8. Kohn-Sham MO representation and energy diagrams of **12a** (left), **12c** (center) and **13d** (right).

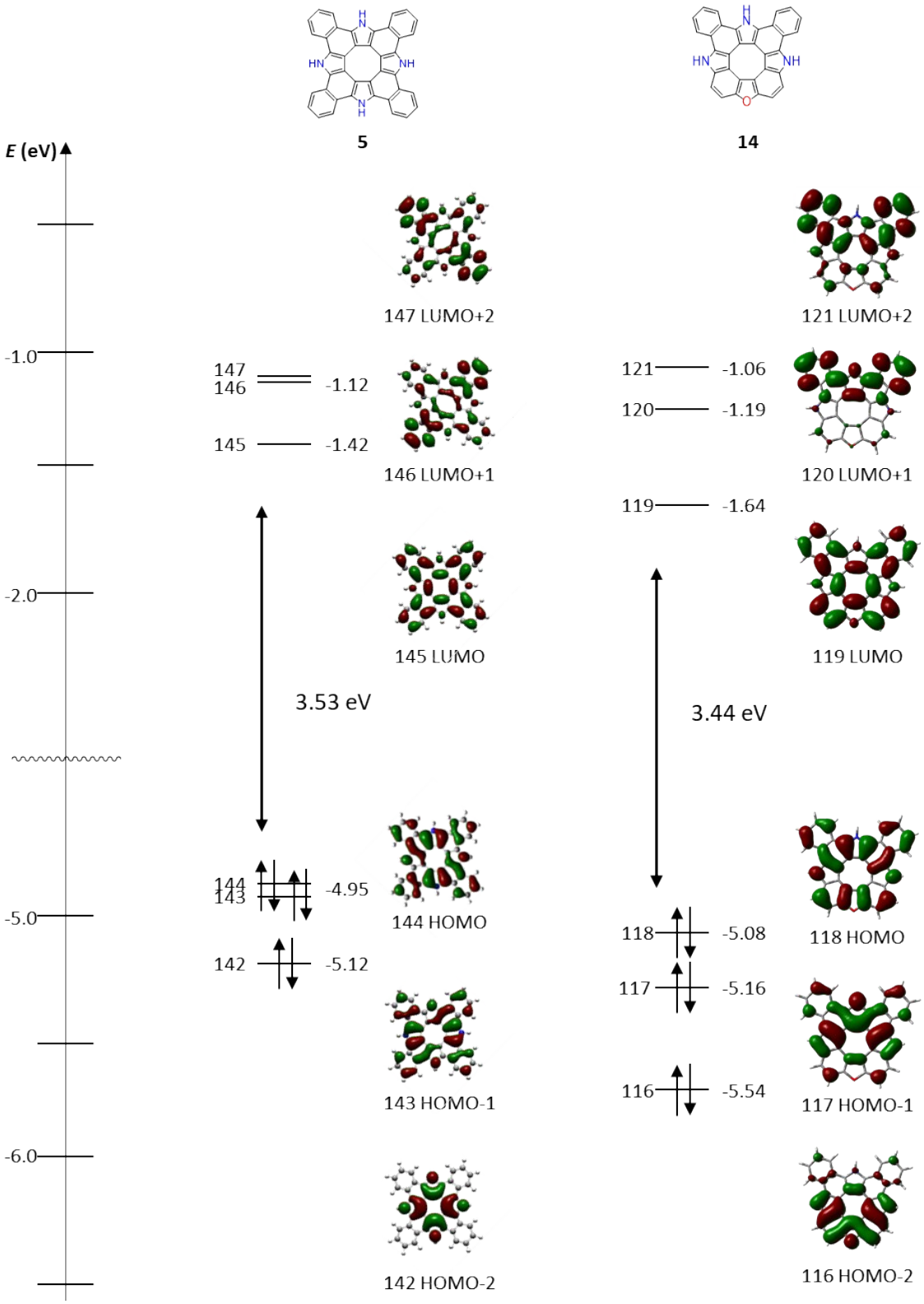

Figure S5-9. Kohn-Sham MO representation and energy diagrams of **5** (left) and **14** (right).

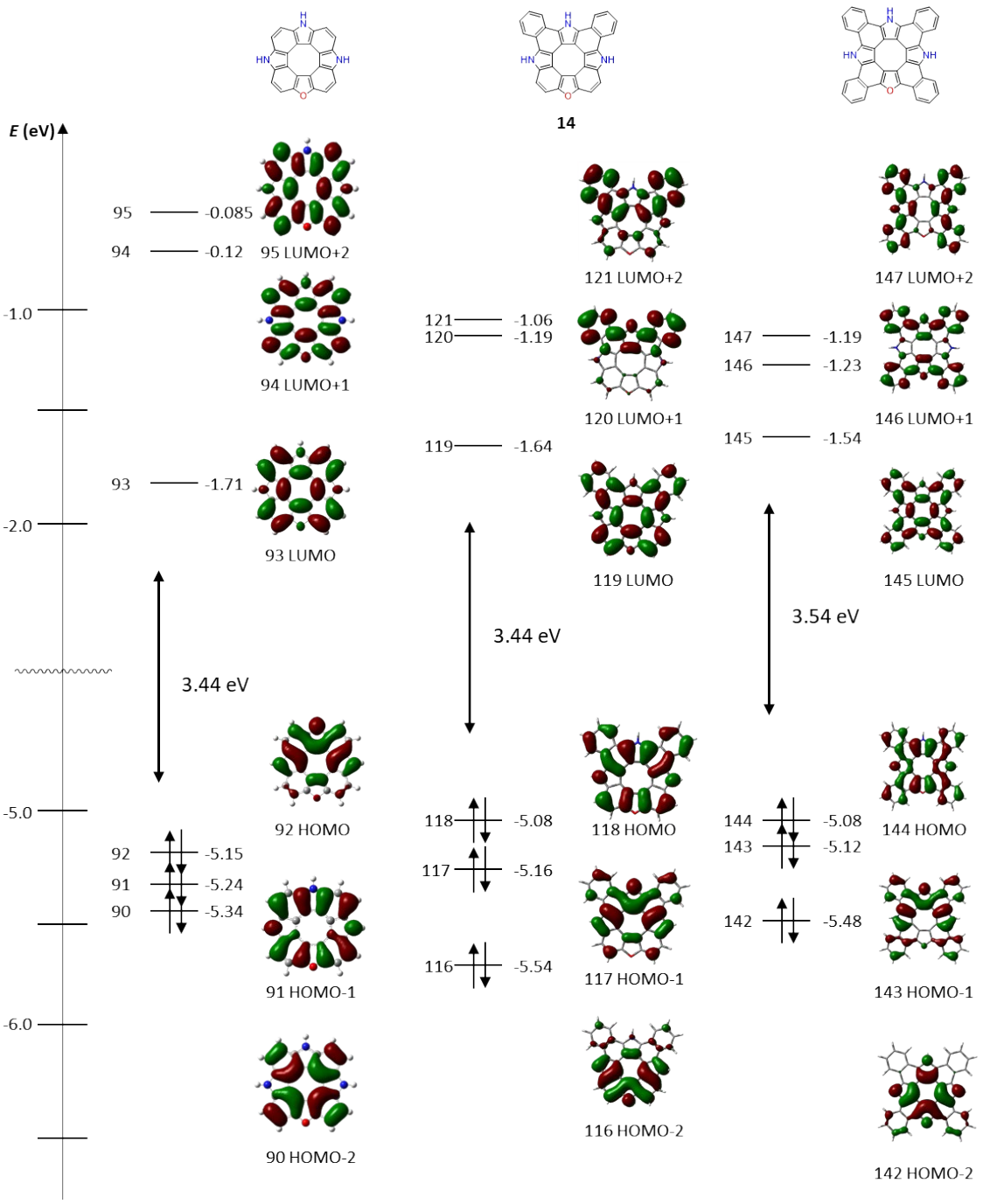

Figure S5-10. Kohn-Sham MO representation and energy diagrams of triazaoxa[8]circulene, dibenzotriazaoxa[8]circulene (left) **14** (center) and tetrabenzotriazaoxa[8]circulene (right).

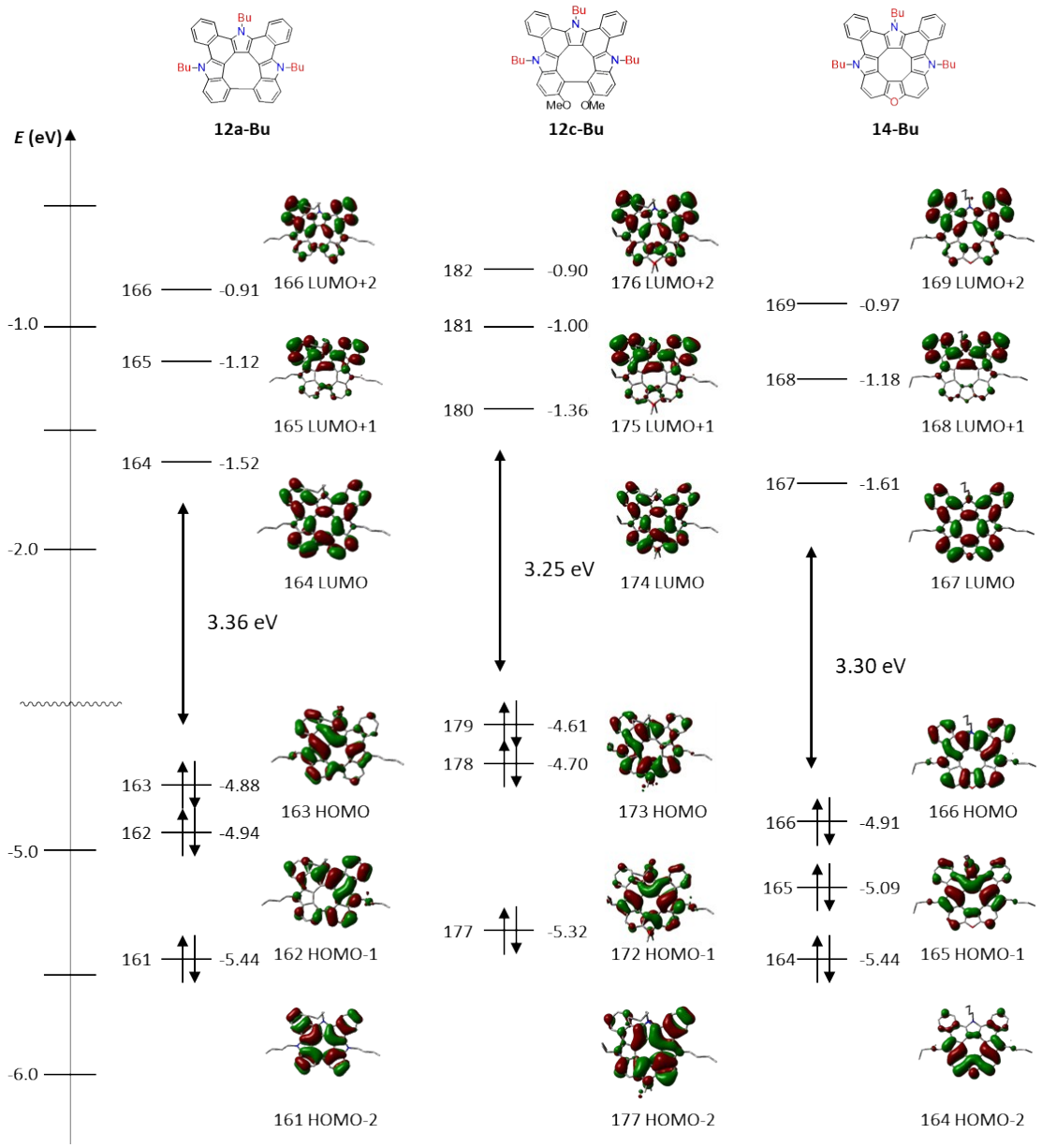

Figure S5-11. Kohn-Sham MO representation and energy diagrams of **12a-Bu** (left), **12c-Bu** (center) and **14-Bu** (right). Hydrogen molecules are omitted for clarity.

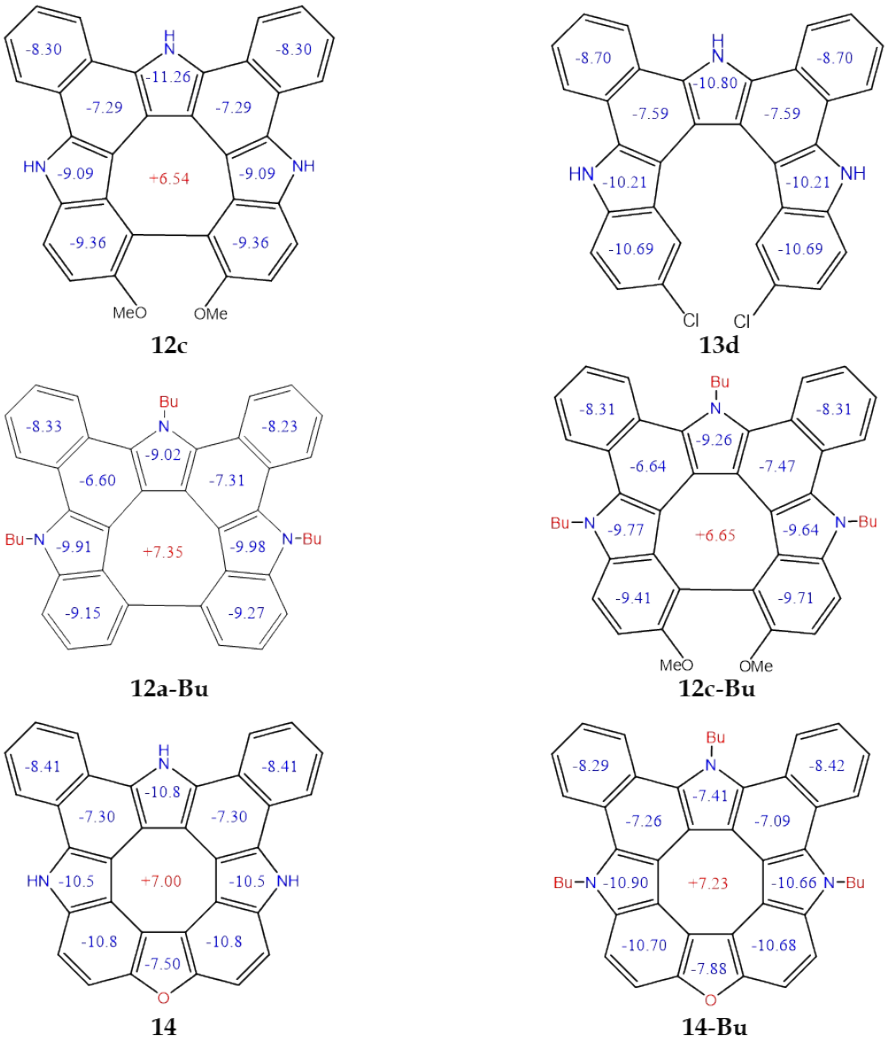

Figure S5-12. Calculated NICS(0)$_{iso}$ values (in ppm) of **12c**, **13d**, **12a-Bu**, **12c-Bu**, **14** and **14-Bu.** The values were calculated at the center of each ring.

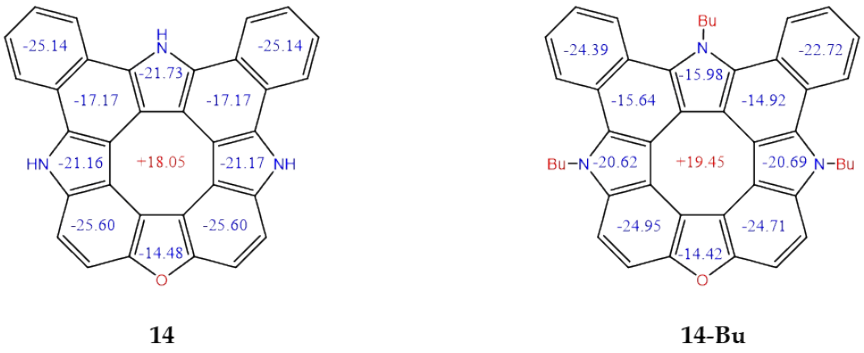

Figure S5-13. Calculated NICS(1)$_{zz}$ values (in ppm) of **14** and **14-Bu.** The values were calculated 1 Å above the center of each ring.

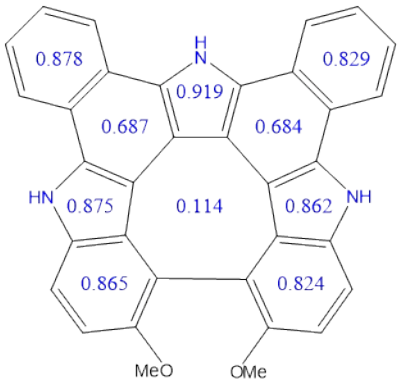

12c

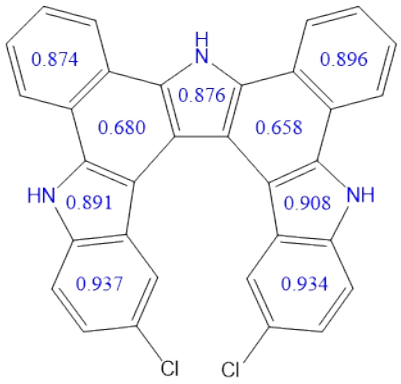

13d

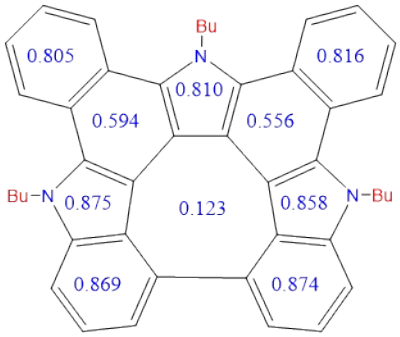

12a-Bu

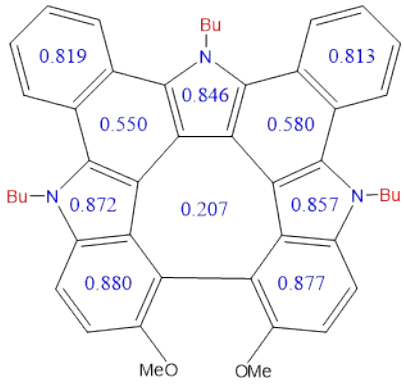

12c-Bu

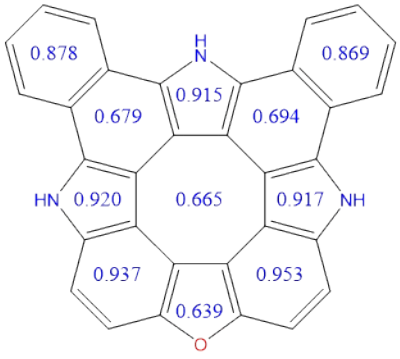

14

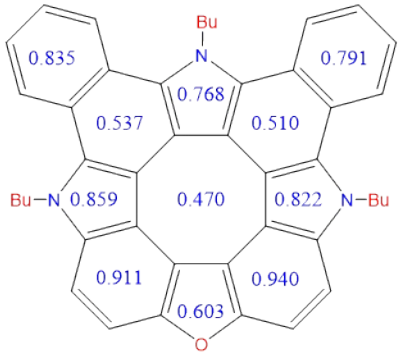

14-Bu

Figure S5-14. Calculated HOMA values[S7,8] of each ring from crystal structures.

6. X-Ray Crystallographic Details

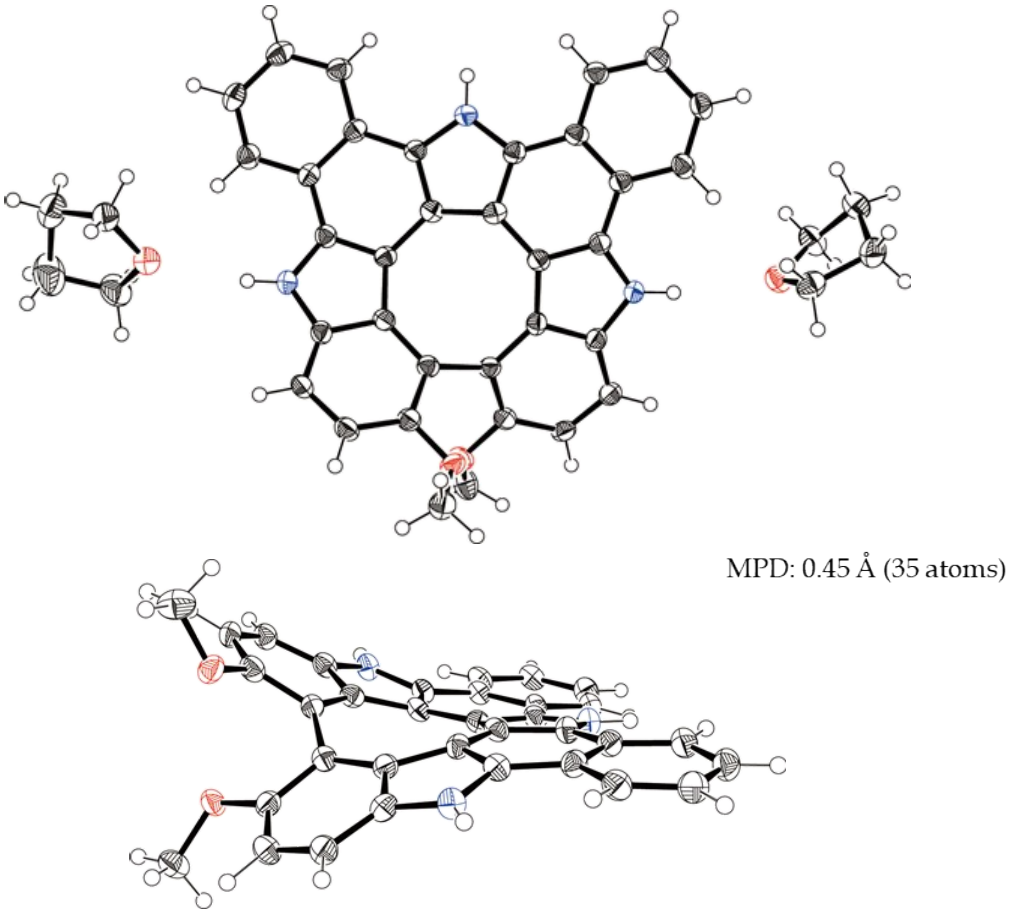

Figure S6-1. X-Ray crystal structure of **12c**. Thermal ellipsoids were scaled to 50% probability.

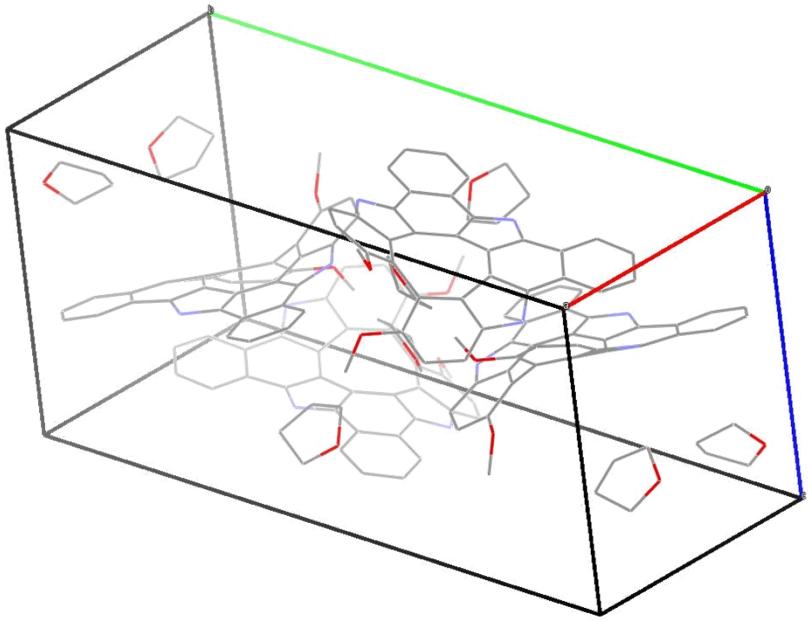

Figure S6-2. Packing structure of **12c**. Hydrogen atoms were omitted for clarity.

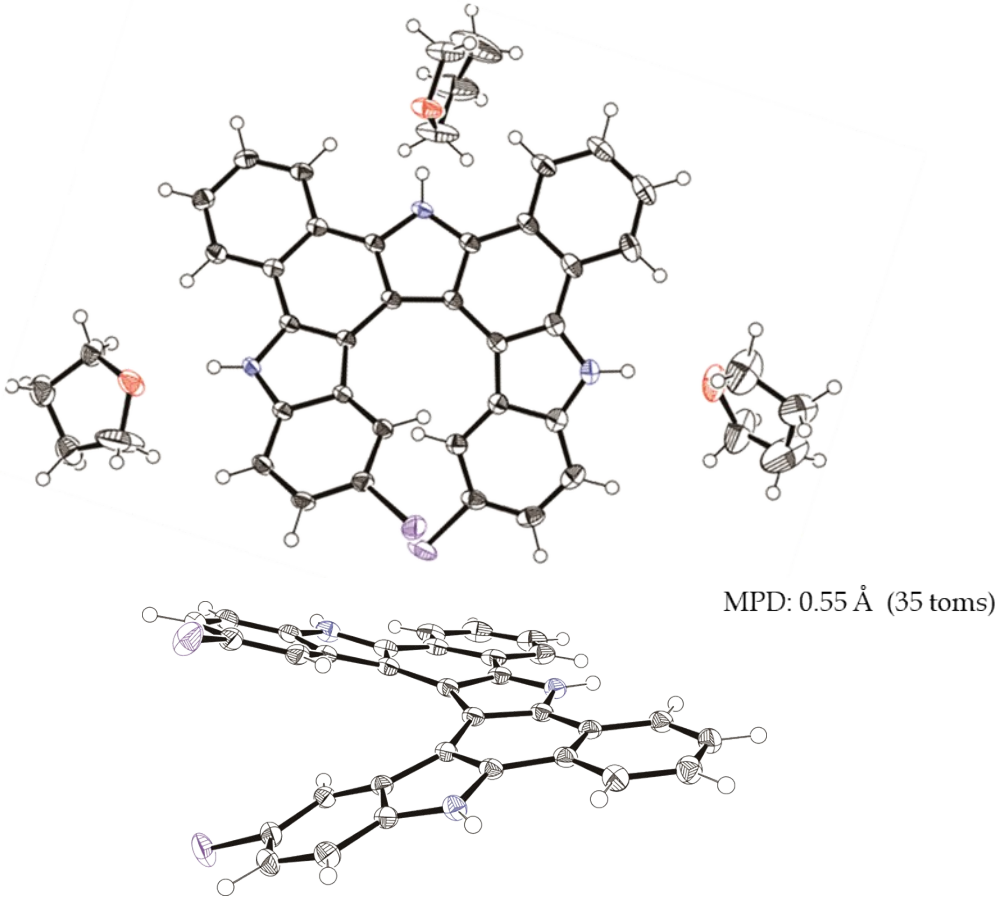

Figure S6-3. X-Ray crystal structure of **13d**. Thermal ellipsoids were scaled to 50% probability.

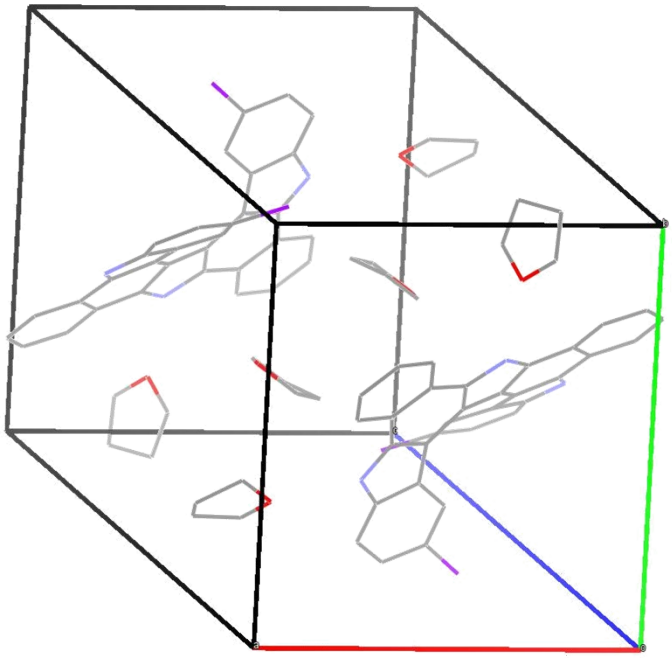

Figure S6-4. Packing structure of **13d**. Hydrogen atoms were omitted for clarity.

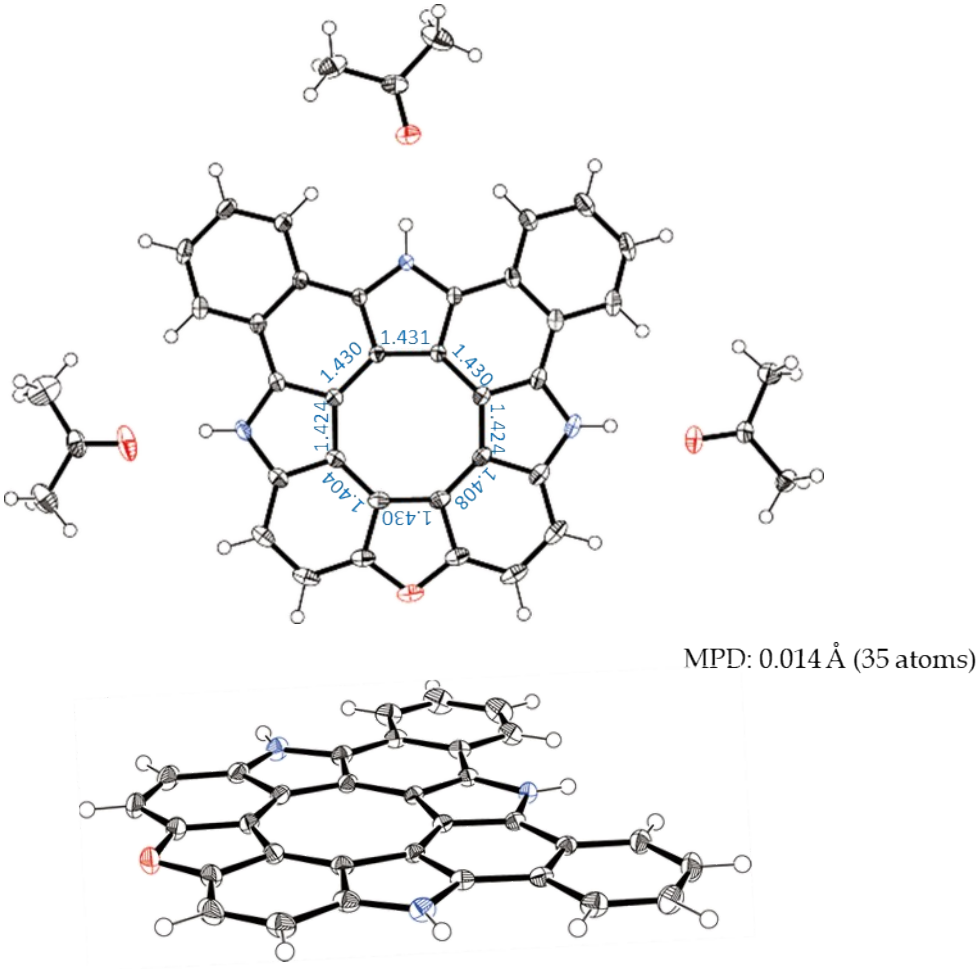

Figure S6-5. X-Ray crystal structure of **14**. Thermal ellipsoids were scaled to 50% probability.

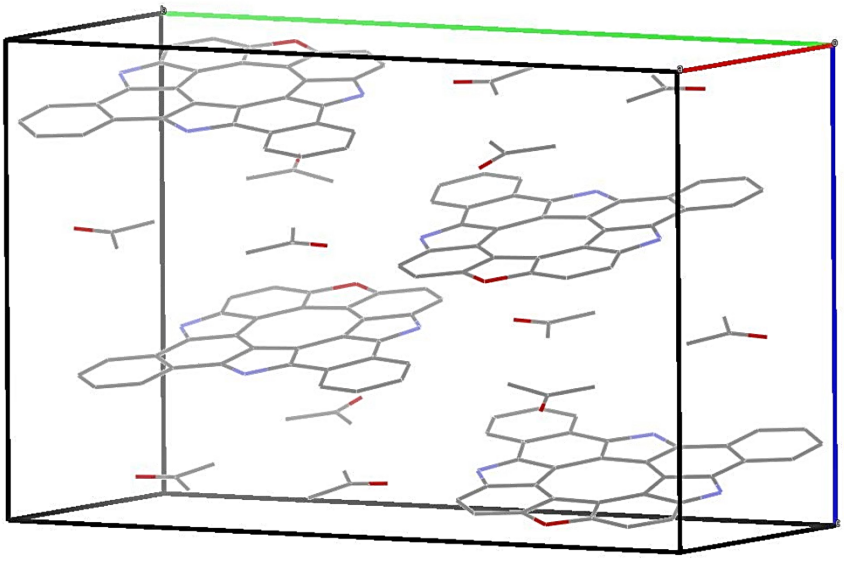

Figure S6-6. Packing structure of **14**. Hydrogen atoms were omitted for clarity.

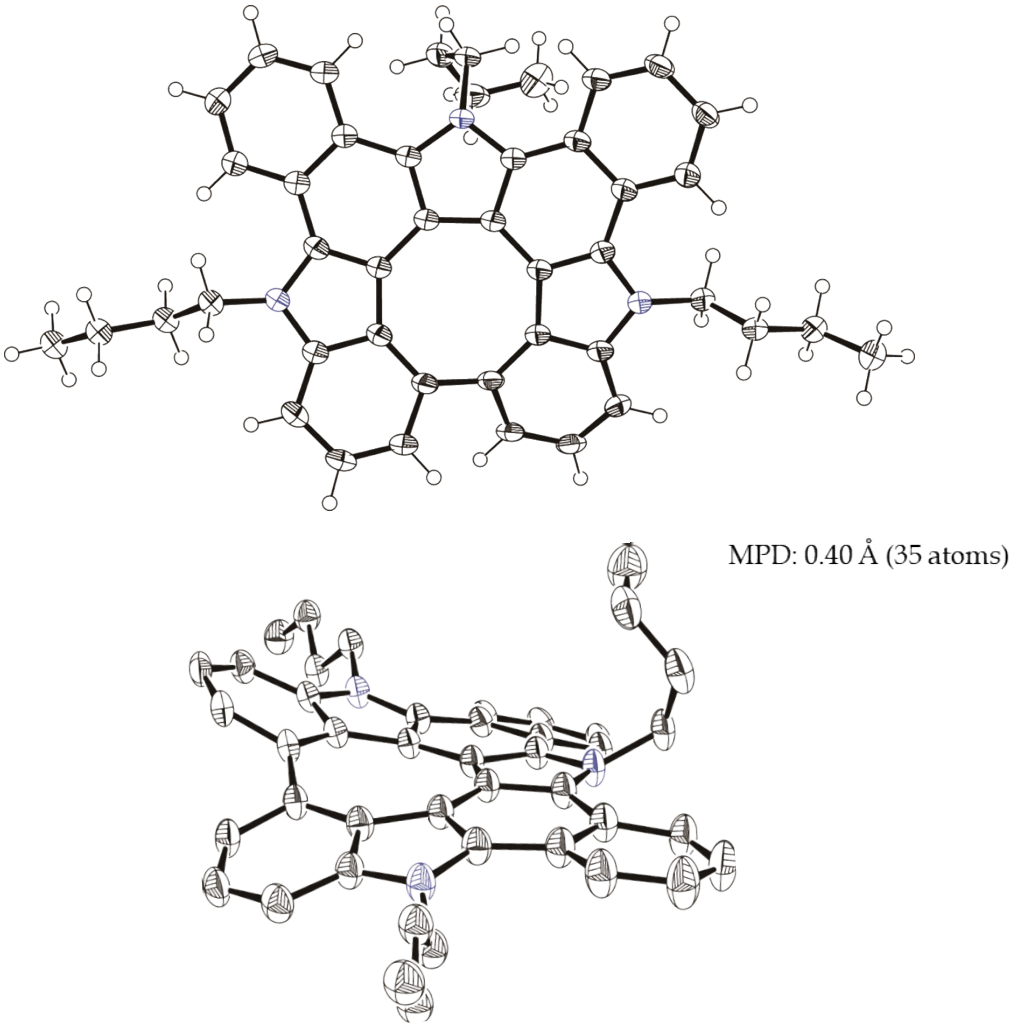

Figure S6-7. X-Ray crystal structure of **12a-Bu**. Thermal ellipsoids were scaled to 50% probability. Solvent molecules omitted for clarity. Hydrogen atoms were omitted for clarity (bottom).

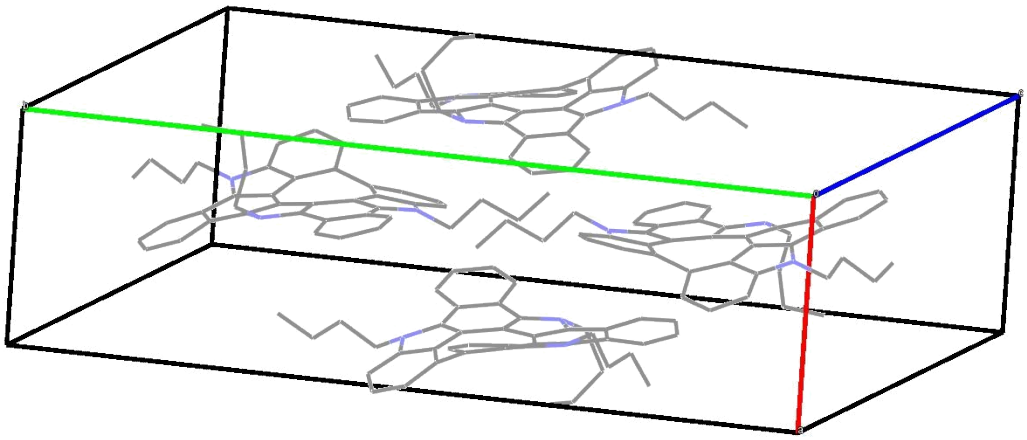

Figure S6-8. Packing structure of **12a-Bu**. Hydrogen atoms were omitted for clarity.

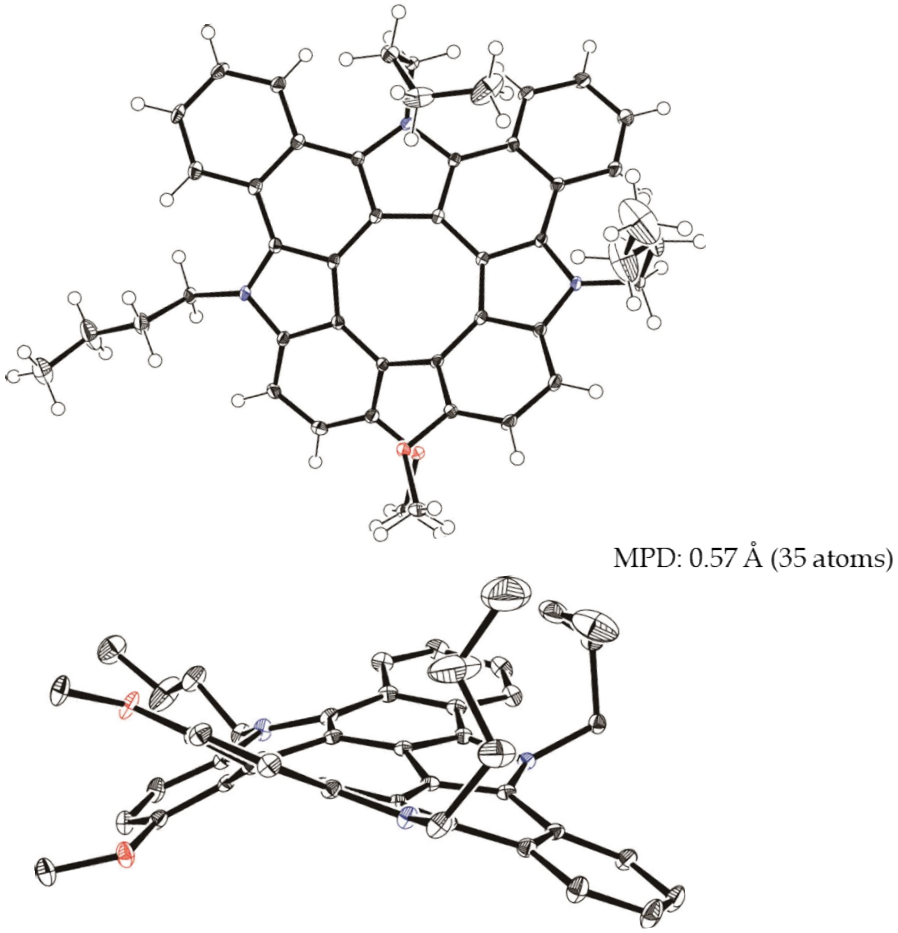

Figure S6-9. X-Ray crystal structure of **12c-Bu**. Thermal ellipsoids were scaled to 50% probability. Solvent molecules omitted for clarity. Hydrogen atoms were omitted for clarity (bottom).

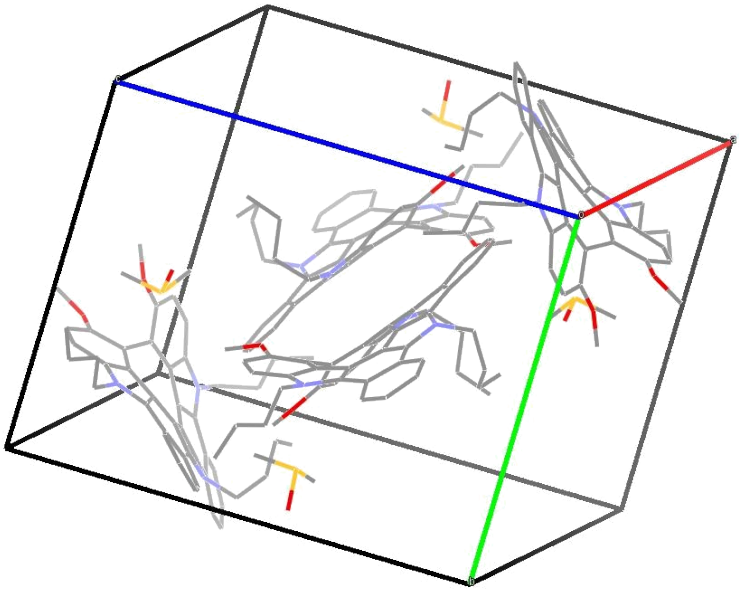

Figure S6-10. Packing structure of **12c-Bu**. Hydrogen atoms were omitted for clarity.

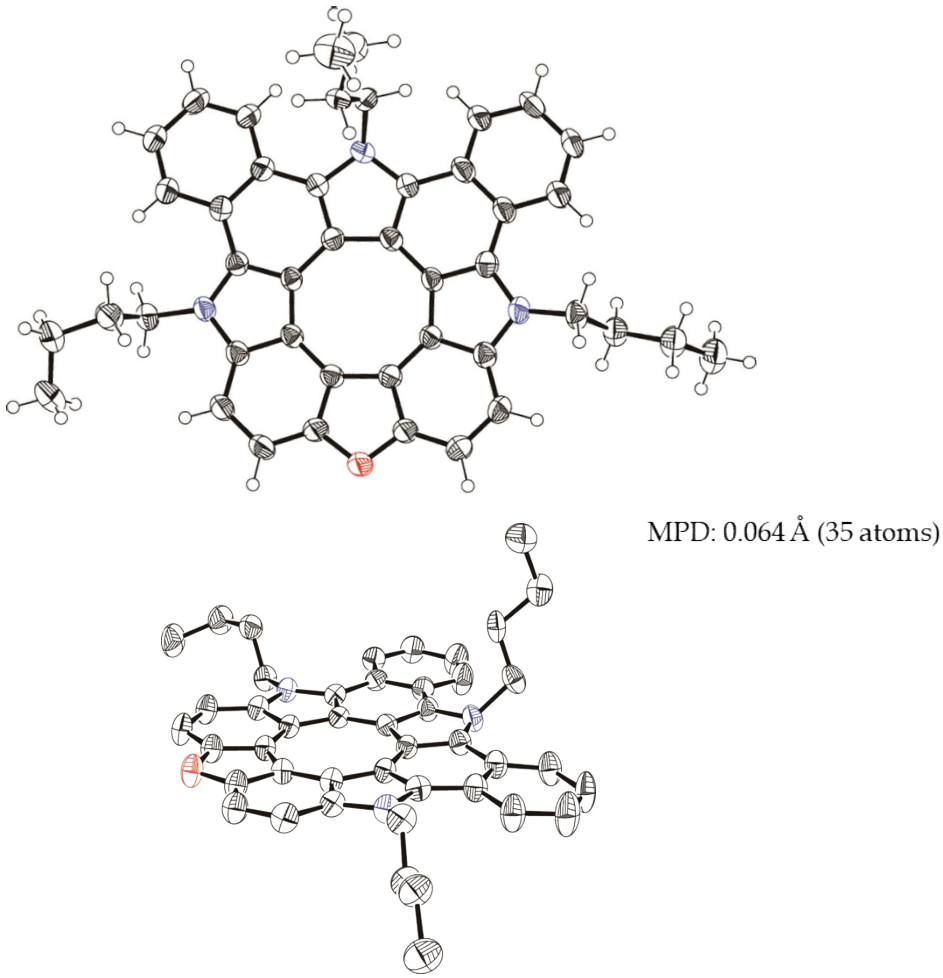

Figure S6-11. X-Ray crystal structure of **14-Bu**. Thermal ellipsoids were scaled to 50% probability. Solvent molecules omitted for clarity. Hydrogen atoms were omitted for clarity (bottom).

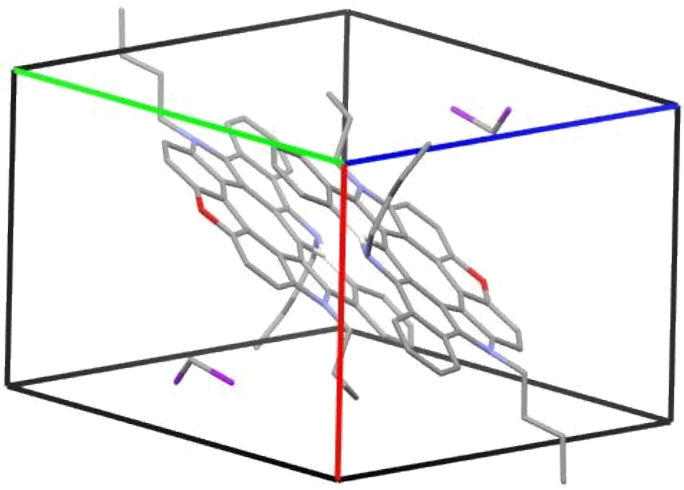

Figure S6-12. Packing structure of **14-Bu**. Hydrogen atoms were omitted for clarity.

Table S6-1. Crystal data and structure refinements for **12c**, **13d** and **14**.

Compound	**12c**	**13d**	**14**
Empirical Formula	$C_{34}H_{21}O_2$, 2(C_4H_8O)	$C_{32}H_{27}N_3Cl_2$, 3(C_4H_8O)	$C_{32}H_{15}N_3O$, 3(C_3H_6O)
M_W	647.78	730.70	631.73
Crystal System	monoclinic	triclinic	monoclinic
Space Group	$P\,2_1/n$ (No. 14)	P -1 (No. 2)	$P\,2_1/c$ (No. 14)
a [Å]	10.5709(4)	12.0391(15)	10.5647(16)
b [Å]	24.7927(5)	12.6294(18)	21.451(4)
c [Å]	11.9563(3)	12.8334(8)	13.969(2)
α [deg]	90	74.367(11)	90
β [deg]	93.905(3)	75.366(11)	91.911(5)
γ [deg]	90	86.809(19)	90
Volume [Å^3]	3126.25(16)	1818.0(4)	3163.9(9)
Z	4	2	4
Density [g/cm^3]	1.376	1.335	1.326
Completeness	0.969	0.979	0.986
Goodness-of-fit	1.082	1.055	1.077
R_1 [$I > 2\sigma(I)$]	0.0887	0.0599	0.0360
wR_2 (all data)	0.3301	0.1563	0.1095
Solvent System	THF/*n*-hexane	THF/*n*-hexane	acetone/*n*-hexane
CCDC No.	1953597	1953596	1953592

Table S6-2. Crystal data and structure refinements for **12a-Bu**, **12c-Bu** and **14-Bu**.

Compound	**12a-Bu**	**12c-Bu**	**14-Bu**
Empirical Formula	$C_{44}H_{41}N_3$	$C_{46}H_{45}N_3O_2$, $2(C_2H_6OS)$	$C_{44}H_{39}N_3O$, CH_2Cl_2
M_W	611.83	828.15	710.75
Crystal System	monoclinic	triclinic	triclinic
Space Group	$P\ 2_1/a$ (No. 14)	P -1 (No. 2)	P -1 (No.2)
a [Å]	8.191(3)	14.877(2)	10.881(4)
b [Å]	35.062(11)	15.0887(14)	13.068(7)
c [Å]	11.513(3)	17.9227(12)	13.624(7)
α [deg]	90	71.320(5)	114.604(18)
β [deg]	107.607(5)	89.990(11)	92.906(5)
γ [deg]	90	89.980(12)	97.348(10)
Volume [Å^3]	3151.6(17)	3811.3(7)	1735.2(14)
Z	4	2	2
Density [g/cm^3]	1.289	1.307	1.356
Completeness	0.982	0.977	0.977
Goodness-of-fit	1.033	1.007	1.010
R_1 [$I > 2\sigma(I)$]	0.0610	0.0638	0.0639
wR_2 (all data)	0.1769	0.1747	0.1754
Solvent System	CH_2Cl_2/*n*-hexane	DMSO/*n*-hexane	CH_2Cl_2/*n*-hexane
CCDC No.	1953593	1953595	1953594

7. UV/Vis Absorption and Emission Spectra

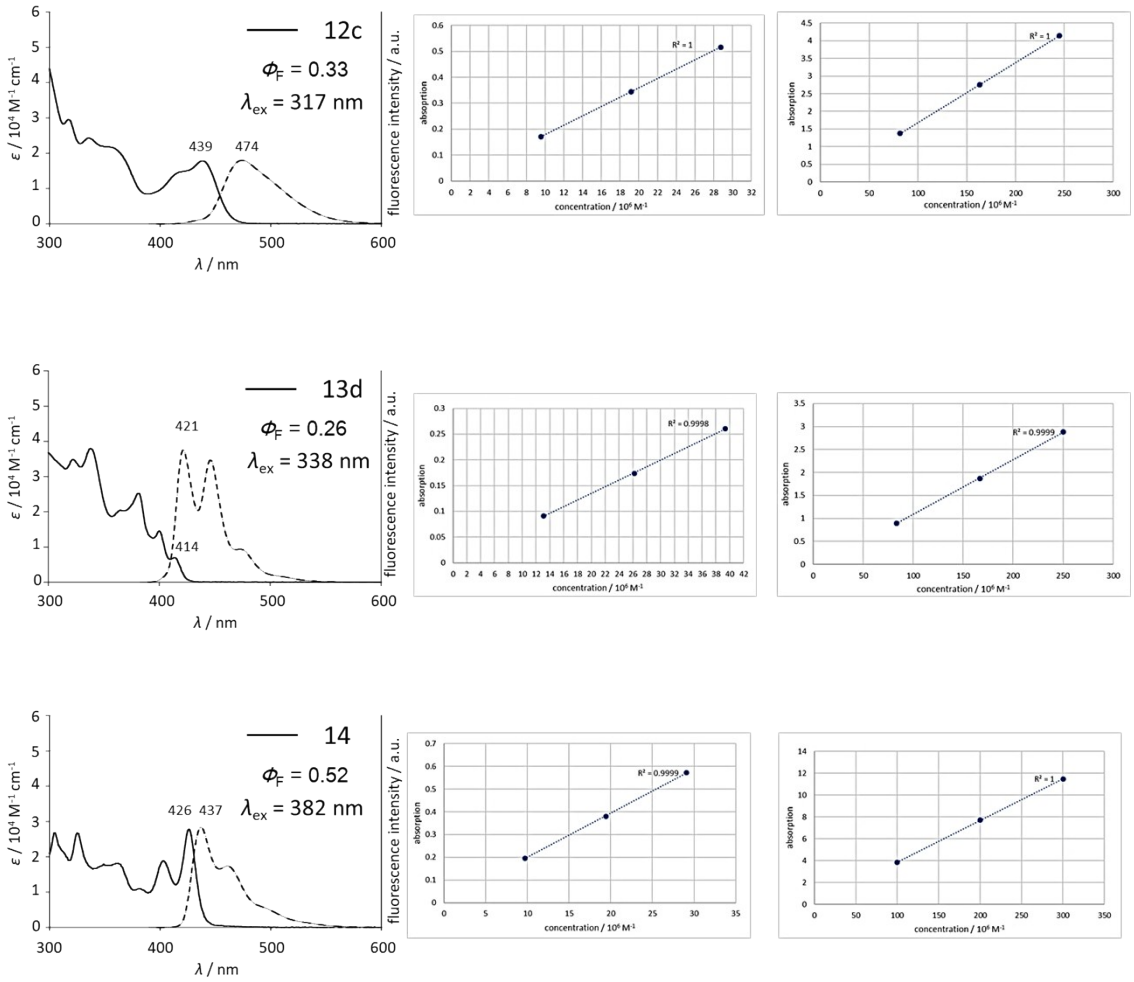

Figure S7-1. UV/Vis absorption and emission spectra of **12c**, **13d** and **14** in THF (left). UV/Vis absorption of **12c** (439 nm), **13d** (400 nm) and **14** (426 nm) in THF (right).

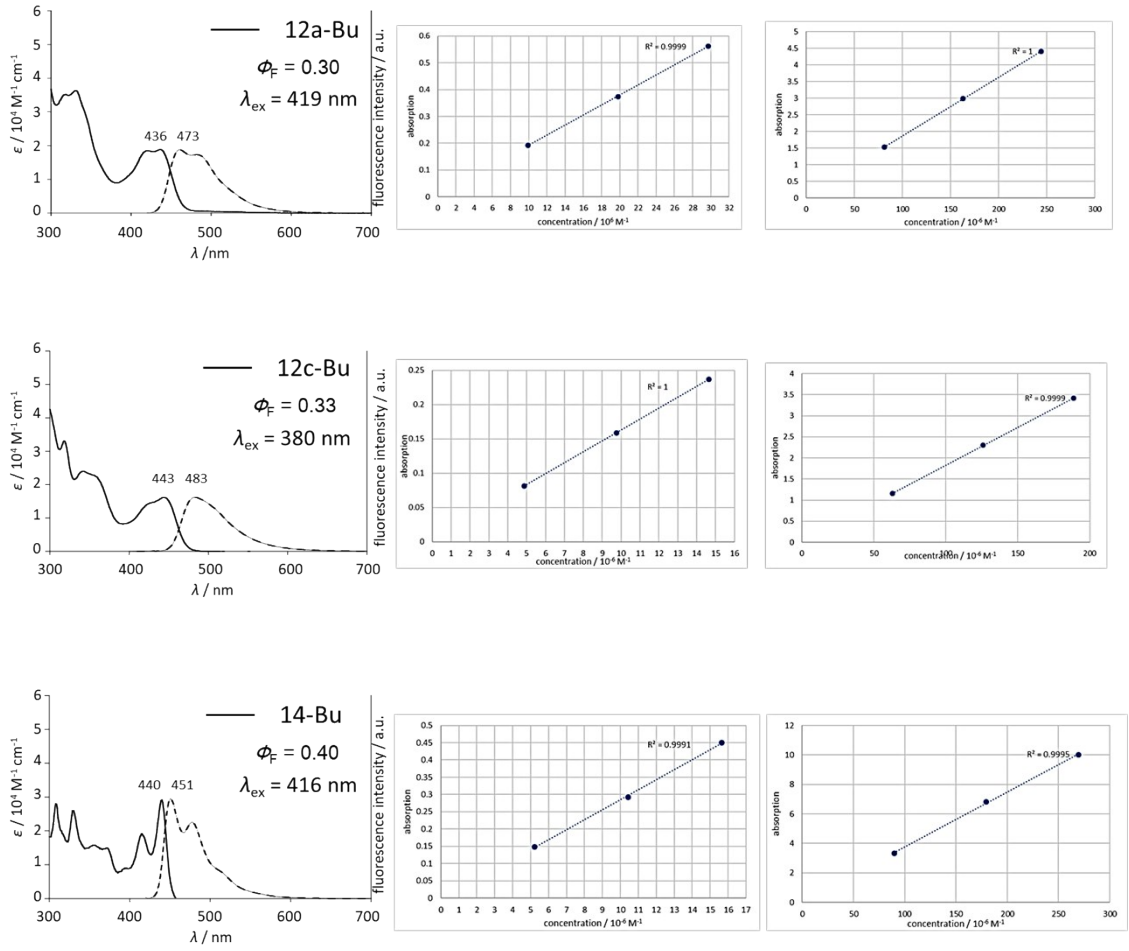

Figure S7-2. UV/Vis absorption and emission spectra of **12a-Bu**, **12c-Bu** and **14-Bu** in THF (left). UV/Vis absorption of **12a-Bu** (436 nm), **12c-Bu** (443 nm) and **14-Bu** (440 nm) in THF (right).

Table S7-1. Summary of the optical properties.

Conpound	λ_{abs}	λ_{ex}	λ_{FL}	Stokes shift
12c	426 nm	382 nm	474 nm	1680 cm^{-1}
13d	414 nm	338 nm	421 nm	400 cm^{-1}
14	426 nm	317 nm	437 nm	590 cm^{-1}
12a-Bu	436 nm	419 nm	473 nm	1790 cm^{-1}
12c-Bu	443 nm	380 nm	483 nm	1870 cm^{-1}
14-Bu	440 nm	416 nm	451 nm	550 cm^{-1}

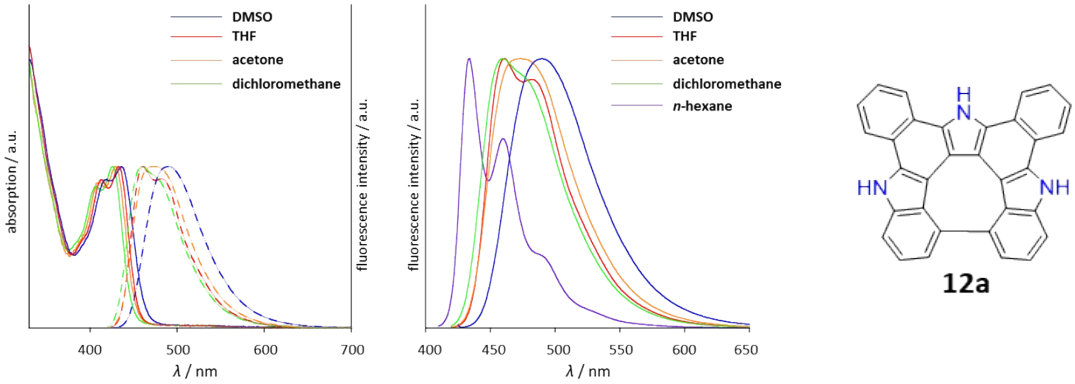

Figure S7-3. Normalized absorption and emission spectra of **12a** in DMSO (blue line), THF (red line), acetone (orange line), dichloromethane (green line) and *n*-hexane (purple line).

Table S7-2. Summary of the optical properties of **12a**.

Solvent	λ_{abs}	λ_{ex}	λ_{FL}	Stokes shift
n-hexane	426 nm	400 nm	434 nm	430 cm^{-1}
THF	433 nm	414 nm	462 nm	1450 cm^{-1}
dichloromethane	426 nm	406 nm	459 nm	1690 cm^{-1}
acetone	429 nm	411 nm	474 nm	2210 cm^{-1}
DMSO	436 nm	419 nm	490 nm	2530 cm^{-1}

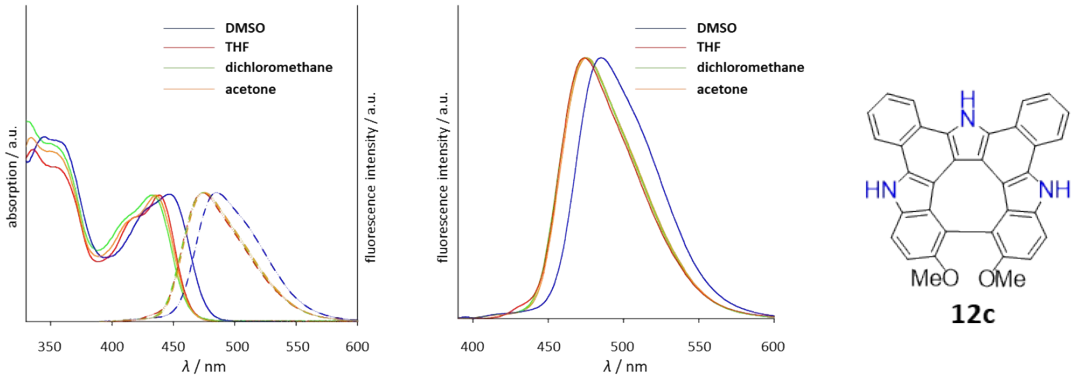

Figure S7-4. Normalized absorption and emission spectra of **12c** in DMSO (blue line), THF (red line), acetone (orange line) and dichloromethane (green line).

Table S7-3. Summary of the optical properties of **12c**.

Solvent	λ_{abs}	λ_{ex}	λ_{FL}	Stokes shift
THF	439 nm	317 nm	474 nm	1680 cm^{-1}
dichloromethane	432 nm	353 nm	475 nm	2100 cm^{-1}
acetone	436 nm	353 nm	476 nm	1930 cm^{-1}
DMSO	444 nm	353 nm	485 nm	1900 cm^{-1}

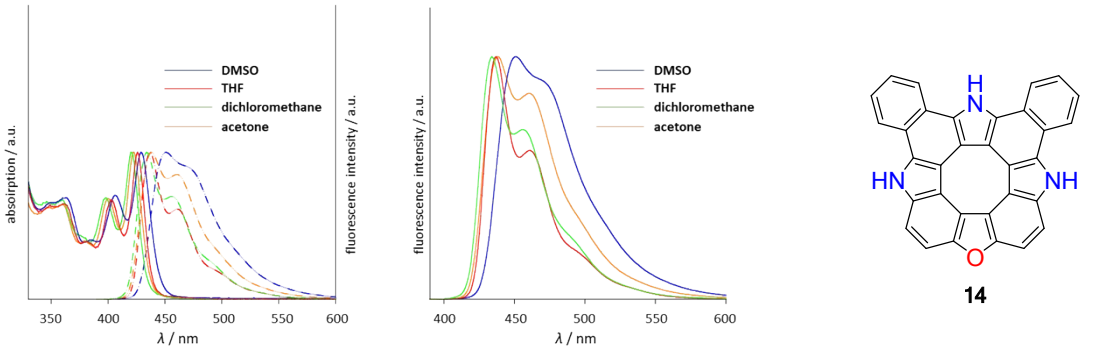

Figure S7-5. Normalized absorption and emission spectra of **14** in DMSO (blue line), THF (red line), acetone (orange line) and dichloromethane (green line).

Table S7-4. Summary of the optical properties of **14**.

Solvent	λ_{abs}	λ_{ex}	λ_{FL}	Stokes shift
THF	426 nm	382 nm	437 nm	590 cm^{-1}
dichloromethane	420 nm	380 nm	434 nm	770 cm^{-1}
acetone	422 nm	360 nm	438 nm	870 cm^{-1}
DMSO	429 nm	360 nm	449 nm	1040 cm^{-1}

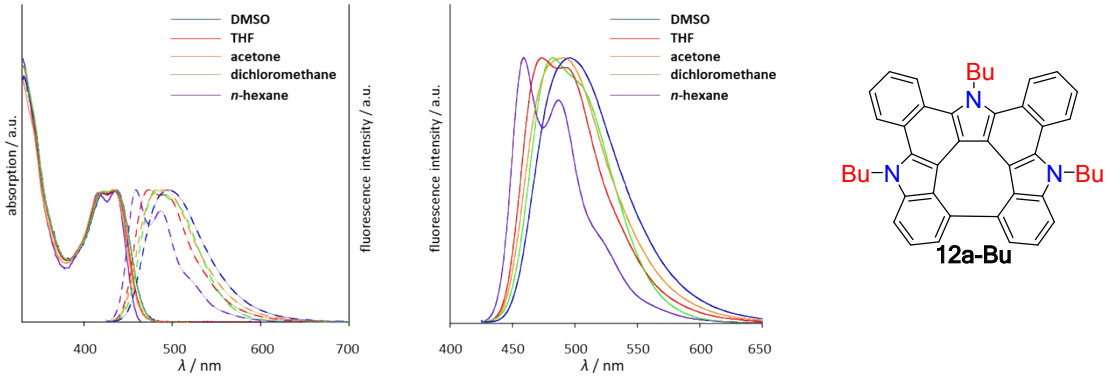

Figure S7-6. Normalized absorption and emission spectra of **12a-Bu** in DMSO (blue line), THF (red line), acetone (orange line), dichloromethane (green line) and *n*-hexane (purple line).

Table S7-5. Summary of the optical properties of **12a-Bu**.

Solvent	λ_{abs}	λ_{ex}	λ_{FL}	Stokes shift
n-hexane	435 nm	414 nm	459 nm	1200 cm^{-1}
THF	436 nm	419 nm	473 nm	1790 cm^{-1}
dichloromethane	436 nm	331 nm	482 nm	2190 cm^{-1}
acetone	432 nm	430 nm	491 nm	2780 cm^{-1}
DMSO	435 nm	420 nm	496 nm	2830 cm^{-1}

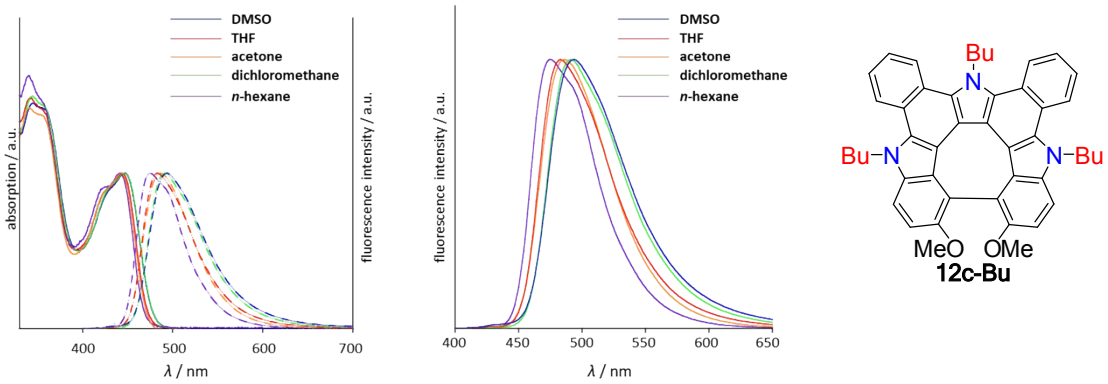

Figure S7-7. Normalized absorption and emission spectra of **12c-Bu** in DMSO (blue line), THF (red line), acetone (orange line), dichloromethane (green line) and *n*-hexane (purple line).

Table S7-6. Summary of the optical properties of **12c-Bu**.

Solvent	λ_{abs}	λ_{ex}	λ_{FL}	Stokes shift
n-hexane	442 nm	430 nm	475 nm	1570 cm^{-1}
THF	443 nm	380 nm	483 nm	1870 cm^{-1}
dichloromethane	447 nm	380 nm	491 nm	2000 cm^{-1}
acetone	443 nm	430 nm	486 nm	2000 cm^{-1}
DMSO	447 nm	380 nm	494 nm	2130 cm^{-1}

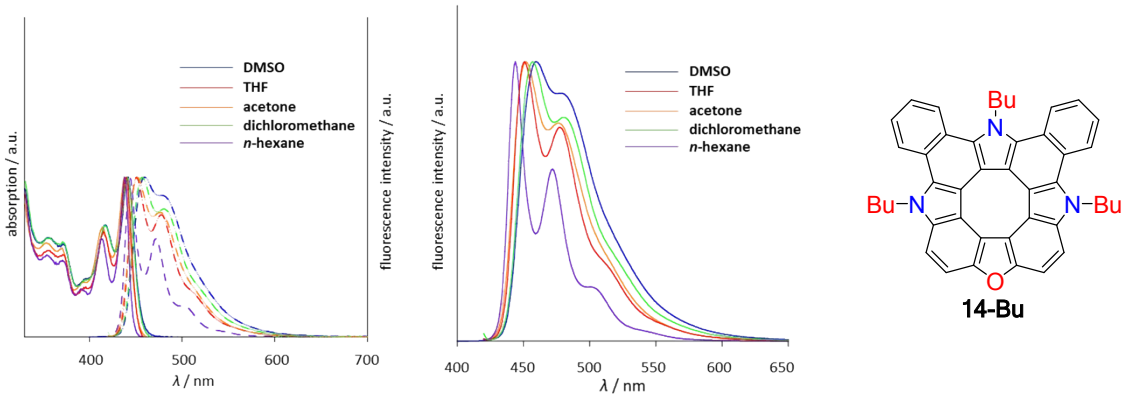

Figure S7-8. Normalized absorption and emission spectra of **14-Bu** in DMSO (blue line), THF (red line), acetone (orange line), dichloromethane (green line) and *n*-hexane (purple line).

Table S7-7. Summary of the optical properties of **14-Bu**.

Solvent	λ_{abs}	λ_{ex}	λ_{FL}	Stokes shift
n-hexane	438 nm	414 nm	444 nm	610 cm^{-1}
THF	440 nm	416 nm	451 nm	550 cm^{-1}
dichloromethane	441 nm	417 nm	457 nm	790 cm^{-1}
acetone	438 nm	414 nm	452 nm	710 cm^{-1}
DMSO	442 nm	417 nm	460 nm	890 cm^{-1}

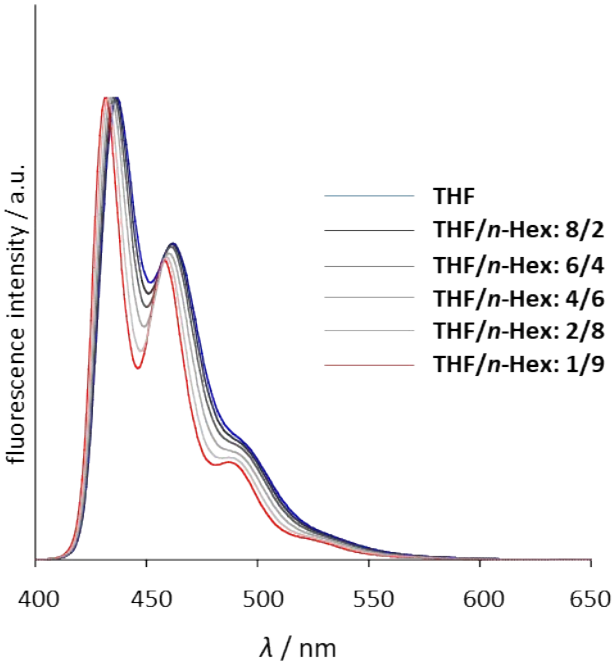

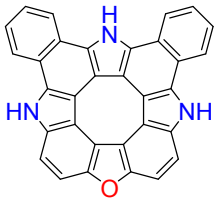

14

Figure S7-9. Normalized fluorescence spectra of **14** in binary solvent system (THF/*n*-hexane).

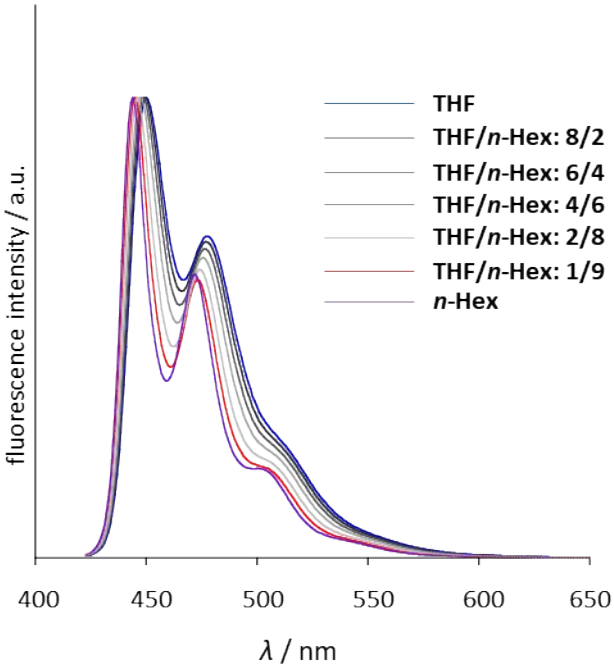

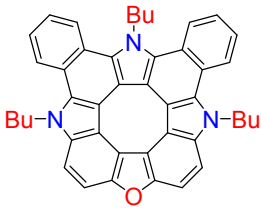

14-Bu

Figure S7-10. Normalized fluorescence spectra of **14-Bu** in binary solvent system (THF/*n*-hexane).

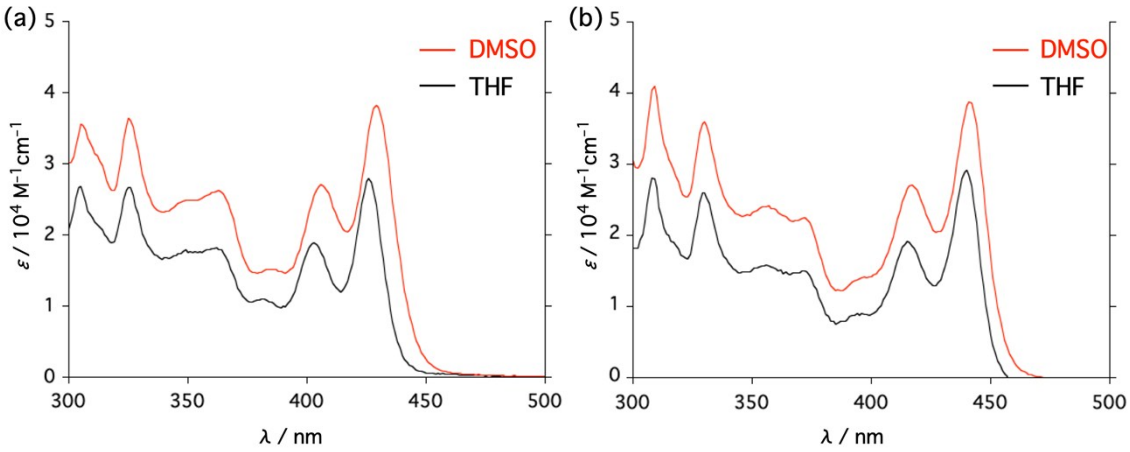

Figure S7-11. UV/Vis absorption spectra of (a) **14** and (b) **14-Bu** in THF (black) and DMSO (red).

8. Fluorescence Lifetime

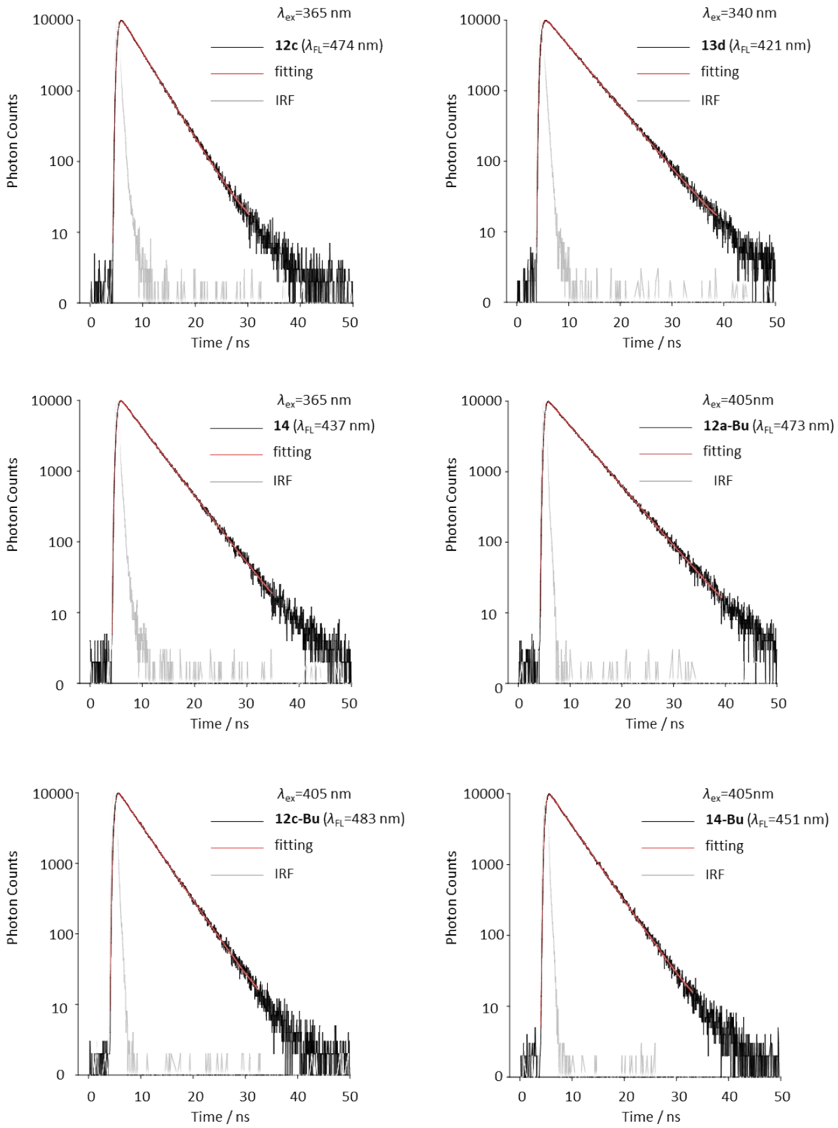

Figure S8-1. Fluorescence decay profiles of **12c**, **13d**, **14**, **12a-Bu**, **12c-Bu** and **14** in THF. (IRF = instrumental response function)

Table S8-1. Summary of the optical properties

compound	λ_{ex}	Φ_F	λ_{FL}	τ_F [ns]	k_r [10^8 s^{-1}]	k_{nr} [10^8 s^{-1}]
12c	317 nm	0.33	476 nm	3.6[a]	0.85	1.9
13d	338 nm	0.26	421 nm	5.0[b]	0.52	1.5
14	325 nm	0.52	437 nm	4.5[a]	1.2	1.1
12a-Bu	419 nm	0.29	473 nm	5.1[c]	0.59	1.4
12c-Bu	443 nm	0.33	491 nm	4.0[c]	0.82	1.7
14-Bu	417 nm	0.40	451 nm	4.1[c]	0.97	1.5

[a] λ_{ex} = 365 nm [b] λ_{ex} = 340 nm [c] λ_{ex} = 405 nm

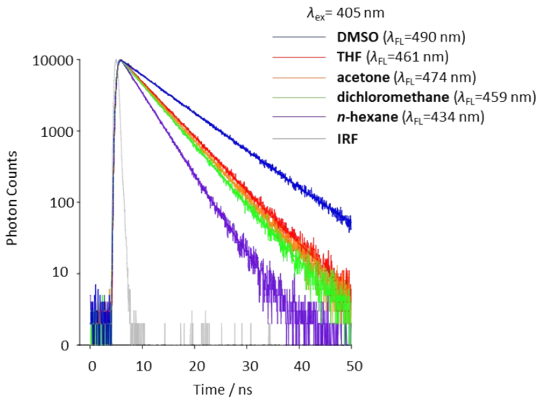

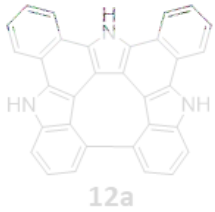

Figure S8-2. Fluorescence decay profiles of **12a** in DMSO (blue line), THF (red line), acetone (orange line), dichloromethane (green line) and *n*-hexane (purple line).

Table S8-2. Summary of optical properties of **12a**.

Solvent	λ_{ex}	Φ_F	λ_{FL}	τ_F[a] [ns]	k_r [10^8 s^{-1}]	k_{nr} [10^8 s^{-1}]
n-hexane	400 nm	0.11	434 nm	3.8	0.30	2.3
acetone	411 nm	0.32	474 nm	5.4	0.59	1.3
dichloromethane	406 nm	0.39	459 nm	5.1	0.75	1.2
THF	412 nm	0.47	461 nm	5.6	0.83	0.93
DMSO	419 nm	0.58	490 nm	8.2	0.71	0.51

[a] λ_{ex} = 405 nm

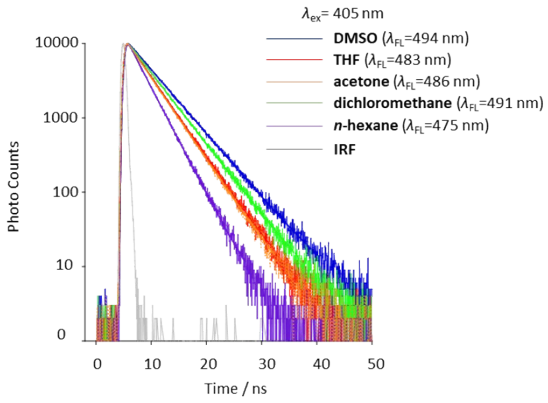

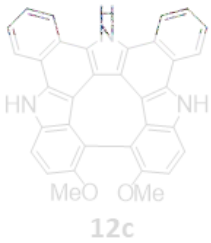

Figure S8-3. Fluorescence decay profiles of **12c** in DMSO (blue line), THF (red line), acetone (orange line) and dichloromethane (green line).

Table S8-3. Summary of optical properties of **12c**.

Solvent	λ_{ex}	Φ_F	λ_{FL}	τ_F[a] [ns]	k_r [10^8 s^{-1}]	k_{nr} [10^8 s^{-1}]
acetone	353 nm	0.29	476 nm	3.4	0.85	2.1
dichloromethane	353 nm	0.37	475 nm	3.4	1.1	1.9
THF	317 nm	0.33	474 nm	3.6	0.92	1.9
DMSO	353 nm	0.49	485 nm	4.6	1.1	1.1

[a] λ_{ex} = 365 nm

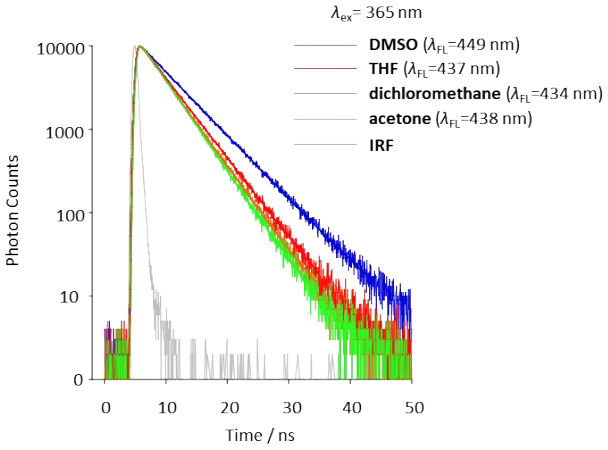

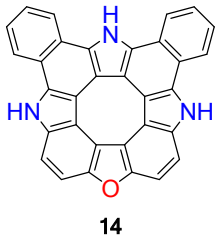

14

Figure S8-4. Fluorescence decay profiles of **14** in DMSO (blue line), THF (red line), acetone (orange line) and dichloromethane (green line).

Table S8-4. Summary of optical properties of **14**.

Solvent	λ_{ex}	Φ_F	λ_{FL}	τ_F[a] [ns]	k_r [10^8 s^{-1}]	k_{nr} [10^8 s^{-1}]
acetone	360 nm	0.45	438 nm	4.2	1.1	1.3
dichloromethane	380 nm	0.39	434 nm	4.0	0.96	1.5
THF	325 nm	0.52	437 nm	4.5	1.2	1.1
DMSO	360 nm	0.72	449 nm	5.7	1.3	0.50

[a] λ_{ex} = 365 nm

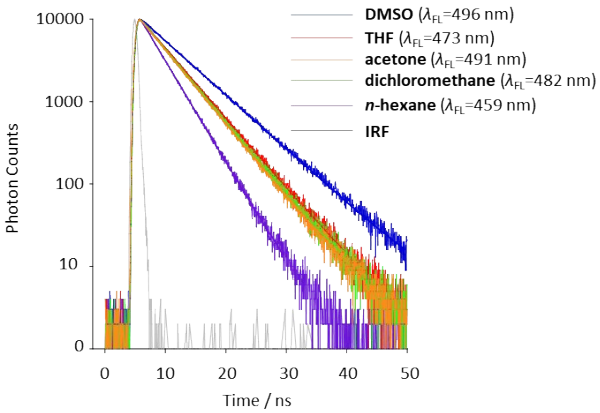

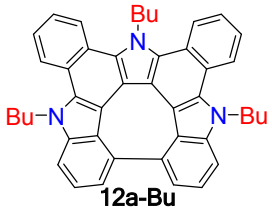

12a-Bu

Figure S8-5. Fluorescence decay profiles of **12a-Bu** in DMSO (blue line), THF (red line), acetone (orange line), dichloromethane (green line) and *n*-hexane (purple line).

Table S8-5. Summary of optical properties of **12a-Bu**.

Solvent	λ_{ex}	Φ_F	λ_{FL}	τ_F[a] [ns]	k_r [10^8 s^{-1}]	k_{nr} [10^8 s^{-1}]
n-hexane	414 nm	0.20	459 nm	3.5	0.58	2.2
acetone	430 nm	0.24	491 nm	4.8	0.49	1.6
dichloromethane	331 nm	0.29	482 nm	4.9	0.60	1.4
THF	419 nm	0.30	473 nm	5.1	0.59	1.4
DMSO	420 nm	0.42	496 nm	6.7	0.62	0.87

[a] λ_{ex} = 405 nm

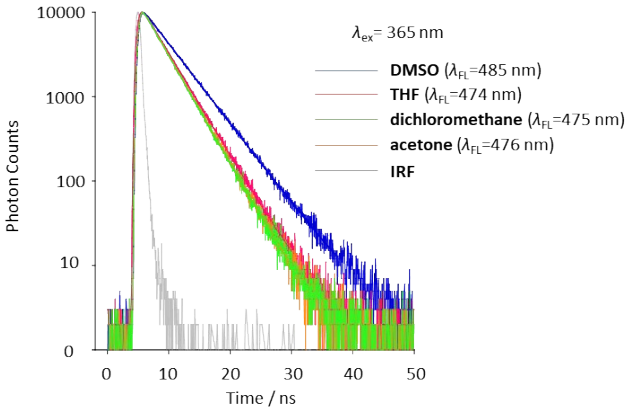

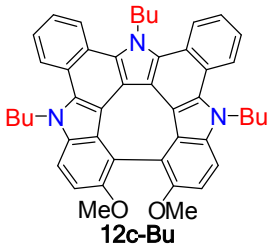

Figure S8-6. Fluorescence decay profiles of **12c-Bu** in DMSO (blue line), THF (red line), acetone (orange line), dichloromethane (green line) and *n*-hexane (purple line).

Table S8-6. Summary of optical properties of **12c-Bu**.

Solvent	λ_{ex}	Φ_F	λ_{FL}	τ_F[a] [ns]	k_r [10^8 s^{-1}]	k_{nr} [10^8 s^{-1}]
n-hexane	430 nm	0.20	475 nm	3.0	0.67	2.7
acetone	430 nm	0.31	486 nm	3.9	0.77	1.8
dichloromethane	447 nm	0.33	483 nm	4.5	0.74	1.5
THF	443 nm	0.33	491 nm	4.0	0.82	1.7
DMSO	447 nm	0.42	494 nm	5.0	0.84	1.2

[a] λ_{ex} = 405 nm

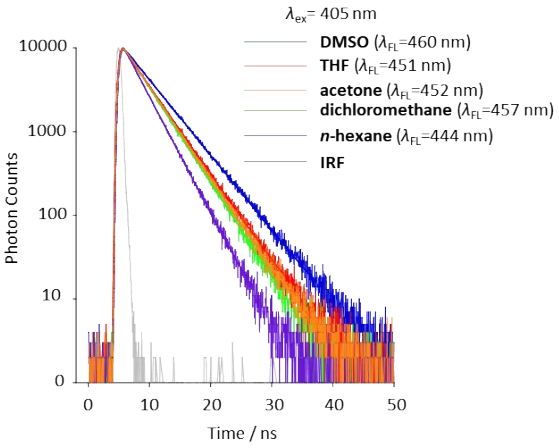

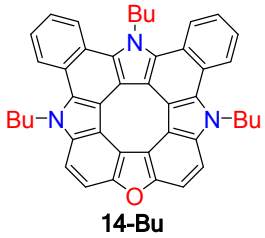

Figure S8-7. Fluorescence decay profiles of **14-Bu** in DMSO (blue line), THF (red line), acetone (orange line), dichloromethane (green line) and *n*-hexane (purple line).

Table S8-7. Summary of optical properties of **14-Bu**.

Solvent	λ_{ex}	Φ_F	λ_{FL}	τ_F[a] [ns]	k_r [10^8 s^{-1}]	k_{nr} [10^8 s^{-1}]
n-hexane	414 nm	0.28	444 nm	3.1	0.89	2.3
acetone	414 nm	0.39	452 nm	3.9	0.98	1.6
dichloromethane	417 nm	0.39	457 nm	3.8	1.0	1.5
THF	416 nm	0.40	451 nm	4.1	0.97	1.5
DMSO	417 nm	0.70	460 nm	4.8	1.5	0.62

[a] λ_{ex} = 405 nm

9. Solubility

The solubilities of **14** and **14-Bu** were measured by the following procedures. (1) A small amount of solvents was added to the solids of each compounds. (2) The resulting suspension was sonicated for 30 sec and the insoluble residue was removed by filtration. (3) The weight of the saturated solution (filtrate) was measured.

Table S9-1. Solubilities of **14** and **14-Bu**

Solvent	acetone	dichloromethane	*n*-hexane	toluene	methanol	diethyl ether	THF
14 (mg/mL)	4.6	0.15	≈ 0	≈ 0	4.2	0.54	21
14-Bu (mg/mL)	5.1	26	0.79	17	1.8	1.7	>79

Figure 9-1. Filtrate of **14** and **14-Bu** in *n*-hexane (left: under room light, right: under UV light).

10. Optical Resolution

Optical separation of **12c-Bu** was performed on a Shimadzu LC-20 AT instrument equipped with a CHIRALPAK IA-3 chiral column (Φ = 4.6 mm). CD spectra were collected on a JASCO J-715 circular dichroism spectrometer at 298 K.

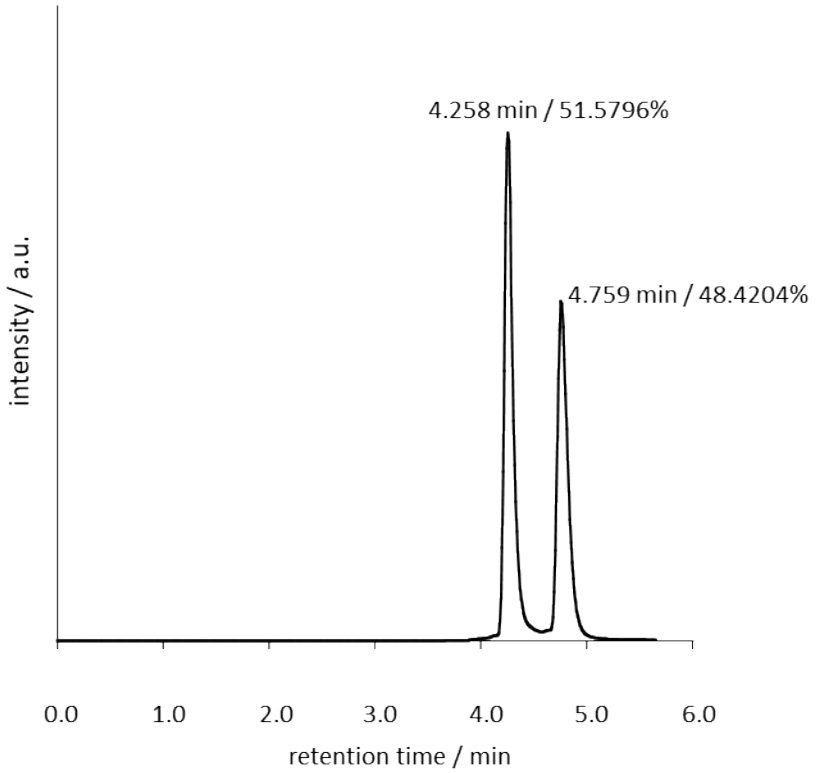

Figure S10-1. Chiral HPLC analysis of **12c-Bu** eluted by dichloromethane using CHIRALPAK IA-3 with a flow rate of 0.9 mL/min.

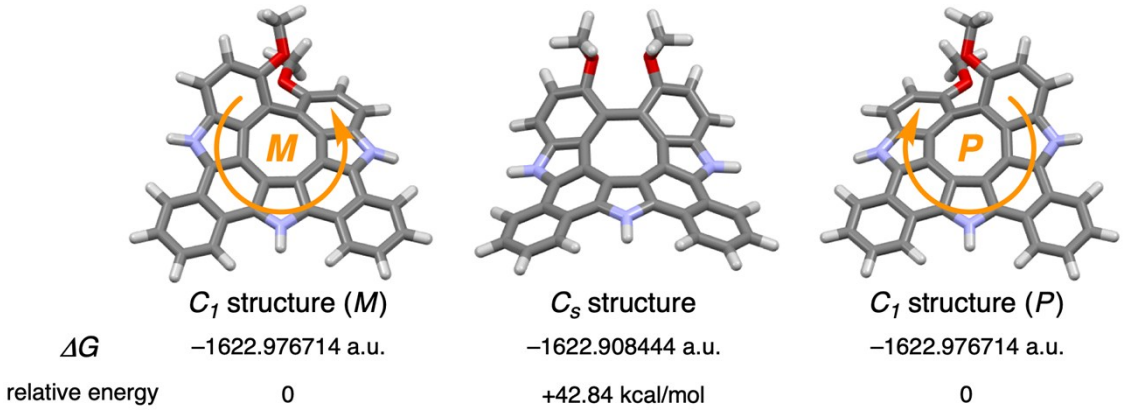

Figure S10-2. Calculated structures of **12c** with C_1 and C_s symmetry restrictions. The calculations were performed at B3LYP/6-311G(d,p) level of theory.

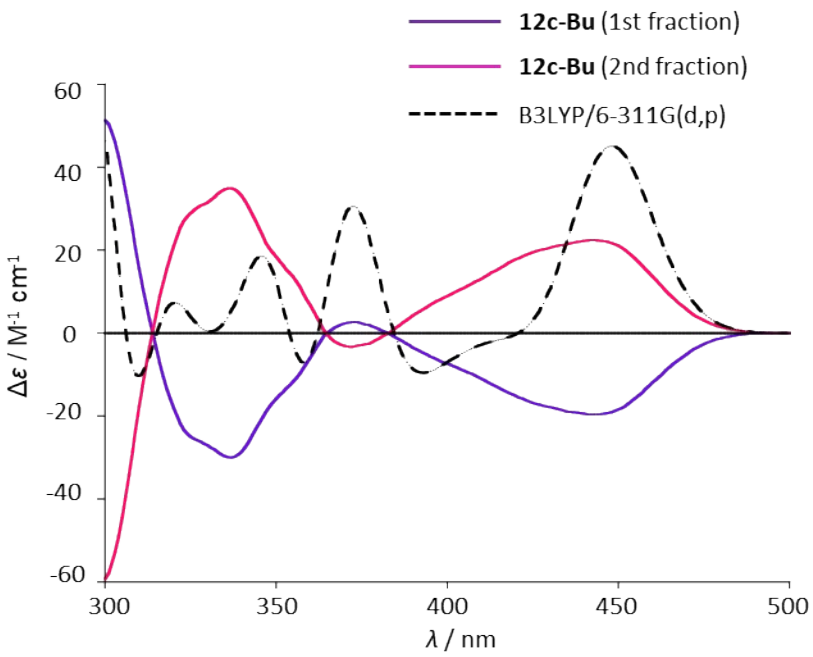

Figure S10-3. Experimental CD spectrum (purple and pink, solid line) in dichloromethane and simulated CD spectrum (black, broken line) of the (*P*)-enantiomer of **12c-Bu** calculated by TD-DFT at the B3YLP/6-311G(d,p) level.

11. Supporting References

[S1] F. Chen, T. Tanaka, T. Mori and A. Osuka, *Chem. Eur. J.*, 2018, **24**, 7489.

[S2] M. E. Hoque, R. Bisht, C. Haldar and B. Chattopadhyay, *J. Am. Chem. Soc.*, 2017, **139**, 7745.

[S3] a) G. M. Sheldrick, *Acta Cryst. A*, 2008, **64**, 112, b) G. M. Sheldrick, *Acta Cryst. C,* 2015, **71**, 3.

[S4] Gaussian 16, Revision A.03, M. J. Frisch, G. W. Trucks, H. B. Schlegel, G. E. Scuseria, M. A. Robb, J. R. Cheeseman, G. Scalmani, V. Barone, G. A. Petersson, H. Nakatsuji, X. Li, M. Caricato, A. V. Marenich, J. Bloino, B. G. Janesko, R. Gomperts, B. Mennucci, H. P. Hratchian, J. V. Ortiz, A. F. Izmaylov, J. L. Sonnenberg, D. Williams-Young, F. Ding, F. Lipparini, F. Egidi, J. Goings, B. Peng, A. Petrone, T. Henderson, D. Ranasinghe, V. G. Zakrzewski, J. Gao, N. Rega, G. Zheng, W. Liang, M. Hada, M. Ehara, K. Toyota, R. Fukuda, J. Hasegawa, M. Ishida, T. Nakajima, Y. Honda, O. Kitao, H. Nakai, T. Vreven, K. Throssell, J. A. Montgomery, Jr., J. E. Peralta, F. Ogliaro, M. J. Bearpark, J. J. Heyd, E. N. Brothers, K. N. Kudin, V. N. Staroverov, T. A. Keith, R. Kobayashi, J. Normand, K. Raghavachari, A. P. Rendell, J. C. Burant, S. S. Iyengar, J. Tomasi, M. Cossi, J. M. Millam, M. Klene, C. Adamo, R. Cammi, J. W. Ochterski, R. L. Martin, K. Morokuma, O. Farkas, J. B. Foresman and D. J. Fox, Gaussian, Inc., Wallingford CT, 2016.

[S5] a) A. D. Becke, *J. Chem. Phys.,* 1993, **98**, 1372. b) C. Lee, W. Yang and R. G. Parr, *Phys. Rev. B*, 1988, **37**, 785.

[S6] H. F. B. Shaidaei, C. S. Wannere, C. Corminboeuf, R. Puchta and P. v. R. Schleyer, *Org. Lett*., 2006, **8**, 863.

[S7] T. M. Krygowski, H. Szatylowicz, O. A. Stasyuk, J. Dominikowska and M. Palusiak, *Chem. Rev.,* 2014, **114**, 6383.